Hyperfine structure and electric quadrupole transitions in the deuterium molecular ion

P. Danev * and D. Bakalov
Institute for Nuclear Research and Nuclear Energy, Bulgarian Academy of Sciences, boulevard Tsarigradsko chaussee 72, Sofia 1142, Bulgaria

V. I. Korobov
Bogoliubov Laboratory of Theoretical Physics, Joint Institute for Nuclear Research, 141980, Dubna, Russia

S. Schiller
Institut für Experimentalphysik, Heinrich-Heine-Universität Düsseldorf, 40225 Düsseldorf, Germany

(Received 26 June 2020; revised 16 December 2020; accepted 17 December 2020; published 11 January 2021)

Molecular hydrogen ions are of metrological relevance due to the possibility of precise theoretical evaluation of their spectrum and of external-field-induced shifts. In homonuclear molecular ions, the electric dipole $E1$ transitions are strongly suppressed, and of primary laser spectroscopy interest is the electric quadrupole ($E2$) transition spectrum. In continuation of previous work on the H_2^+ ion, we report here the results of the calculations of the hyperfine structure of the laser-induced electric quadrupole transitions between a large set of rovibrational states of D_2^+; the inaccuracies of previous evaluations have been corrected. The effects of the laser polarization are studied in detail. We show that the electric quadrupole moment of the deuteron can in principle be determined with low fractional uncertainty ($\simeq 1 \times 10^{-4}$) by comparing the results presented here with future data from precision spectroscopy of D_2^+.

DOI: 10.1103/PhysRevA.103.012805

I. INTRODUCTION

Molecular hydrogen ions (MHIs) are three-body systems that offer unique possibilities for both high-precision spectroscopy and accurate theoretical evaluation of the spectrum (see, e.g., Refs. [1–7] and references therein). The comparison of high-precision experimental and theoretical results opens room for independent tests of QED and has the potential to provide accurate values of fundamental constants. Among the most impressive achievements along this path is the recent determination of the proton-to-electron mass ratio with factional accuracy of $\approx 2 \times 10^{-11}$ from rotational [4] and rovibrational [7] precision laser spectroscopy of cooled and trapped HD^+ ions; also confirmed were the recent adjustments in the CODATA18 (Committee on Data for Science and Technology 2018 [8]) values of the proton charge radius and the Rydberg constant. Transitions with low sensitivity to external fields are considered as promising candidates for the search for a time variation of the mass ratios [1,2].

In the homonuclear MHIs H_2^+, D_2^+, the electric dipole transitions are strongly suppressed and the spectra are dominated by the electric quadrupole transitions, which are much weaker and have much smaller natural width. While precision laser spectroscopy of $E2$ transitions in homonuclear MHIs is still in the future, the theory has achieved significant progress. The first calculations of $E2$ spectra in the approximation of spinless particles, performed back in 1953 by Bates and Poots [9], were followed by works of Posen *et al.* [10], Pilon and Baye [11], and Pilon [12] with ever-increasing precision. The hyperfine structure (HFS) of the $E2$ spectral lines of H_2^+ was first considered in Ref. [2]; in Ref. [13], the leading effects of order $O(m_e\alpha^6)$ were also included in a systematical investigation of the spectrum.

The HFS of the lower excited states of D_2^+ has been previously investigated in Refs. [14–16]. Only a few experimental studies of the HFS of D_2^+ have been carried out until now [17,18].

Babb [19] and Zhang *et al.* [14] raised an interesting question about the possibility of determining Q_d from the hyperfine structure of D_2^+; there is now an intense discussion on its actual value. Recently, Alighanbari *et al.* [6] determined Q_d with fractional uncertainty $u_r(Q_d) = 1.5\%$ from the hyperfine spectrum of a pure rotational transition of HD^+. However, the most precise determination so far is from a comparison of experiment and theory for the neutral hydrogen molecules [20–22]. Their stated uncertainties, ranging from 1×10^{-4} to 8×10^{-4}, are so small that it is worthwhile to perform an independent measurement, using the molecular hydrogen ion HD^+ or D_2^+.

In the present work, we apply the approach of Ref. [13] to the deuterium ion D_2^+. In Sec. II, we re-evaluate the HFS of D_2^+ in the Breit-Pauli approximation by correcting inaccuracies in the preceding works. Section III is dedicated to the study of the laser-stimulated $E2$ transition spectrum in D_2^+ with account of the HFS of the molecular levels and the polarization of the laser source.

In Sec. III D, we demonstrate that the results presented here provide the theoretical input for the composite frequency method [1,6,23] needed to determine the deuteron quadrupole moment from precision spectroscopy of D_2^+ with an

*petar_danev@abv.bg

uncertainty comparable with the uncertainty of the latest values reported in Refs. [20,24].

In the final Sec. IV, we summarize and discuss the results.

II. HYPERFINE STRUCTURE OF DEUTERIUM MOLECULAR ION

A. Theoretical model

The nonrelativistic Hamiltonian of the hydrogen molecular ion $D_2{}^+$ is

$$H^{\rm NR} = \frac{\mathbf{p}_1^2}{2m_d} + \frac{\mathbf{p}_2^2}{2m_d} + \frac{\mathbf{p}_e^2}{2m_e} + \frac{e^2}{4\pi\varepsilon_0}\left(-\frac{1}{r_1} - \frac{1}{r_2} + \frac{1}{r_{12}}\right), \tag{1}$$

where m_d and m_e are the masses of the deuterons and the electron; $\mathbf{R}_1, \mathbf{R}_2, \mathbf{R}_e$ and $\mathbf{p}_1, \mathbf{p}_2, \mathbf{p}_e$ are the position and momentum vectors of the two deuterons and the electron in the center of mass frame; and $\mathbf{r}_{1,2} = \mathbf{R}_e - \mathbf{R}_{1,2}$, $\mathbf{r}_{12} = \mathbf{R}_2 - \mathbf{R}_1$, and $r_{1,2} = |\mathbf{r}_{1,2}|$, $r_{12} = |\mathbf{r}_{12}|$. We consider only Σ_g states of $D_2{}^+$; in the nonrelativistic approximation the discrete Σ_g states of the hydrogen isotope molecular ions are labeled with the quantum numbers of the nuclear vibrational excitation v, of the total orbital momentum L, and of its projection on the space-fixed quantization axis L_z; the spatial parity $\lambda = \pm 1$ is constrained to $\lambda = (-1)^L$ and will be omitted in further notations. The nonrelativistic (Coulomb) energy levels and wave functions of $D_2{}^+$ in the state $|vLL_z\rangle$ are denoted by $E^{({\rm NR})vL}$ and $\Psi^{({\rm NR})vLL_z}$, respectively.

The leading-order spin effects are described by adding to $H^{\rm NR}$ the pairwise spin interaction terms V of the Breit-Pauli Hamiltonian of Ref. [25]:

$$H = H^{\rm NR} + V, \quad V = V_{ed_1} + V_{ed_2} + V_{dd}, \tag{2}$$

where d_1 and d_2 denote the two deuterium nuclei of $D_2{}^+$. We remind readers of the explicit form of the spin interaction operators; to comply with the established traditions, we shall use atomic units $\hbar = e = 4\pi\varepsilon_0 = 1$ in the remainder of Sec. II A:

$$\begin{aligned} V_{ed_1} = \alpha^2\Bigg[&-\frac{4\pi}{3}\mu_e\mu_d\frac{m_e}{m_p}\delta(\mathbf{r}_1)(\mathbf{s}_e\cdot\mathbf{I}_1) + \left(\mu_e - \frac{1}{2}\right)\frac{1}{r_1^3}(\mathbf{r}_1\times\mathbf{p}_e)\cdot\mathbf{s}_e - \mu_e\frac{m_e}{m_d}\frac{1}{r_1^3}(\mathbf{r}_1\times\mathbf{p}_1)\cdot\mathbf{s}_e \\ &- \frac{m_e}{2m_d}\left(\mu_d\frac{m_e}{m_p} - \frac{m_e}{m_d}\right)\frac{1}{r_1^3}(\mathbf{r}_1\times\mathbf{p}_1)\cdot\mathbf{I}_1 + \mu_d\frac{m_e}{2m_p}\frac{1}{r_1^3}(\mathbf{r}_1\times\mathbf{p}_e)\cdot\mathbf{I}_1\Bigg] \\ &+ \alpha^2\left[\mu_e\mu_d\frac{m_e}{2m_p}\frac{r_1^2(\mathbf{s}_e\cdot\mathbf{I}_1) - 3(\mathbf{r}_1\cdot\mathbf{s}_e)(\mathbf{r}_1\cdot\mathbf{I}_1)}{r_1^5}\right] + \frac{Q_d}{2a_0^2}\frac{r_1^2\mathbf{I}_1^2 - 3(\mathbf{r}_1\cdot\mathbf{I}_1)^2}{r_1^5}, \end{aligned} \tag{3}$$

$$V_{ed_2} = V_{ed_1}(\mathbf{r}_1\to\mathbf{r}_2, \mathbf{p}_1\to\mathbf{p}_2, \mathbf{I}_1\to\mathbf{I}_2), \tag{4}$$

$$\begin{aligned} V_{dd} = \alpha^2\Bigg[&-\frac{2\pi}{3}\mu_d^2\frac{m_e^2}{m_p^2}\delta(\mathbf{r}_{12})(\mathbf{I}_1\cdot\mathbf{I}_2) + \frac{\mu_d m_e^2}{2m_p m_d}\left(\frac{1}{r_{12}^3}(\mathbf{r}_{12}\times\mathbf{p}_1)\cdot\mathbf{I}_2 - \frac{1}{r_{12}^3}(\mathbf{r}_{12}\times\mathbf{p}_2)\cdot\mathbf{I}_1\right) \\ &+ \frac{m_e}{2m_d}\left(\mu_d\frac{m_e}{m_p} - \frac{m_e}{m_d}\right)\left(\frac{1}{r_{12}^3}(\mathbf{r}_{12}\times\mathbf{p}_1)\cdot\mathbf{I}_1 - \frac{1}{r_{12}^3}(\mathbf{r}_{12}\times\mathbf{p}_2)\cdot\mathbf{I}_2\right)\Bigg] \\ &+ \alpha^2\left[\mu_d^2\frac{m_e^2}{4m_p^2}\frac{r_{12}^2(\mathbf{I}_1\cdot\mathbf{I}_2) - 3(\mathbf{r}_{12}\cdot\mathbf{I}_1)(\mathbf{r}_{12}\cdot\mathbf{I}_2)}{r_{12}^5}\right] - \frac{Q_d}{2a_0^2}\sum_{i=1,2}\frac{r_{12}^2\mathbf{I}_i^2 - 3(\mathbf{r}_{12}\cdot\mathbf{I}_i)^2}{r_{12}^5}. \end{aligned} \tag{5}$$

Here $\mathbf{I}_{1,2}$ and $\mathbf{s}_e$ are the spin operators of the two deuterons and of the electron, respectively, and proper symmetrization of the terms containing noncommuting operators is assumed; μ_e is the magnetic dipole moment of the electron in units $\mu_0 = e\hbar/2m_e$ (Bohr magneton), μ_d is the magnetic dipole moment of the deuteron in units $\mu_N = e\hbar/2m_p$ (nuclear magneton), a_0 is the Bohr radius, and Q_d is the electric quadrupole moment of the deuteron.

The same spin-interaction Hamiltonian was used in Ref. [14].

The spin interactions split the degenerate nonrelativistic energy levels $E^{({\rm NR})vL}$ into a manifold of hyperfine levels that are distinguished with additional quantum numbers (QNs) describing their "spin composition."

As evidenced in Sec. II C, the appropriate angular momentum coupling scheme for $D_2{}^+$ is

$$\mathbf{I} = \mathbf{I}_1 + \mathbf{I}_2, \quad \mathbf{F} = \mathbf{I} + \mathbf{s}_e, \quad \mathbf{J} = \mathbf{L} + \mathbf{F}.$$

Accordingly, the hyperfine states are labeled with the exact QNs of the total angular momentum J and its projection J_z, and the approximate QNs I, F, and L.

Similar to Refs. [13,14,25], in first order of perturbation theory the hyperfine levels $E^{(vL)IFJJ_z}$ may be put in the form $E^{(vL)IFJJ_z} = E^{({\rm NR})vL} + \Delta E^{(vL)IFJJ_z}$, where the corrections $\Delta E^{(vL)IFJJ_z}$, also referred to as "hyperfine energies" or "hyperfine shifts," are the eigenvalues of the effective spin interaction Hamiltonian $H^{\rm eff}$. (Of course, in the absence of external fields the energies are degenerate in J_z.)

Instead of the above, however, we shall use the more general form

$$E^{(vL)IFJJ_z} = E^{({\rm diag})vL} + \Delta E^{(vL)IFJJ_z}, \tag{6}$$

where $E^{({\rm diag})vL}$ also includes the relativistic, QED, etc. spin-independent corrections to the nonrelativistic energy levels $E^{({\rm NR})vL}$.

Since the evaluation of $\Delta E^{(vL)IFJ}$ is the point where our results disagree to some extent with the results of Refs. [14,15], we give more details of the calculations.

B. Effective spin Hamiltonian

We associate with the spin of the deuteron d_1 the $(2I_1+1)$-dimensional space of the irreducible representation (I_1) of $su(2)$ with basis vectors $|I_1 I_{1z}\rangle$, $I_{1z} = -I_1, \ldots, I_1$, satisfying

$$\hat{\mathbf{I}}_1^2 |I_1 I_{1z}\rangle = I_1(I_1+1)|I_1 I_{1z}\rangle, \quad \hat{I}_{1z}|I_1 I_{1z}\rangle = I_{1z}|I_1 I_{1z}\rangle.$$

Similarly, we define the sets $|I_2 I_{2z}\rangle$, $|s_e s_{ez}\rangle$, and $|LL_z\rangle$. The basis set $|IFF_z\rangle$ in the resulting space of the spin variables of all $D_2{}^+$ constituents is taken in the form

$$|IFF_z\rangle = \sum_{I_{1z}I_{2z}s_{ez}I_z} C^{II_z}_{I_1 I_{1z}, I_2 I_{2z}} C^{FF_z}_{II_z, s_e s_{ez}} |I_1 I_{1z}\rangle |I_2 I_{2z}\rangle |s_e s_{ez}\rangle, \tag{7}$$

where $C^{LM}_{l_1 m_1, l_2 m_2} = \langle l_1 l_2 m_1 m_2 | LM\rangle$ are Clebsch-Gordan coefficients. Thus, the basis set in the hyperfine manifold of the (vL) state of $D_2{}^+$ consists of the functions

$$\Psi_0^{(vL)IFJJ_z} = \sum_{L_z F_z} C^{JJ_z}_{LL_z, FF_z} \Psi^{(\mathrm{NR})vLL_z} |IFF_z\rangle. \tag{8}$$

We also define a basis set depending on the angular part only, which will be referred to as "pure" states,

$$|LIFJJ_z\rangle = \sum_{L_z, F_z} C^{JJ_z}_{LL_z, FF_z} |LL_z\rangle |IFF_z\rangle. \tag{9}$$

The effective spin Hamiltonian H^{eff} is a matrix operator acting on the finite-dimensional space spanned by the vectors $|LIFJJ_z\rangle$, such that

$$H^{\mathrm{eff}\,(vL)J}_{I'F',IF} \equiv \langle LI'F'JJ_z | H^{\mathrm{eff}} | LIFJJ_z\rangle = \left\langle \Psi_0^{(vL)I'F'JJ_z} \middle| V \middle| \Psi_0^{(vL)IFJJ_z} \right\rangle. \tag{10}$$

In the absence of external fields, the matrix of $H^{\mathrm{eff}\,(vL)J}_{I'F',IF}$ is independent of J_z. For the deuterium molecular ion, H^{eff} has the form

$$\begin{aligned} H^{\mathrm{eff}} &= E_1(\mathbf{L}\cdot\mathbf{s}_e) + E_2(\mathbf{L}\cdot\mathbf{I}) + E_3(\mathbf{I}\cdot\mathbf{s}_e) + E_4(2\mathbf{L}^2(\mathbf{I}\cdot\mathbf{s}_e) - 3[(\mathbf{L}\cdot\mathbf{I})(\mathbf{L}\cdot\mathbf{s}_e) + (\mathbf{L}\cdot\mathbf{s}_e)(\mathbf{L}\cdot\mathbf{I})] \\ &\quad + E_5(2\mathbf{L}^2(\mathbf{I}_1\cdot\mathbf{I}_2) - 3[(\mathbf{L}\cdot\mathbf{I}_1)(\mathbf{L}\cdot\mathbf{I}_2) + (\mathbf{L}\cdot\mathbf{I}_2)(\mathbf{L}\cdot\mathbf{I}_1)]) \\ &\quad + E_6\big(\mathbf{L}^2\mathbf{I}_1^2 - \tfrac{3}{2}(\mathbf{L}\cdot\mathbf{I}_1) - 3(\mathbf{L}\cdot\mathbf{I}_1)^2 + \mathbf{L}^2\mathbf{I}_2^2 - \tfrac{3}{2}(\mathbf{L}\cdot\mathbf{I}_2) - 3(\mathbf{L}\cdot\mathbf{I}_2)^2\big). \end{aligned} \tag{11}$$

Compared to the effective spin Hamiltonian for $H_2{}^+$ of Ref. [13], H^{eff} of Eq. (11) includes one additional term (with E_6, last line) that describes the effects due to the electric quadrupole moment of the nuclei and arises when averaging the last term in Eqs. (3)–(5). The first four terms in Eq. (11) coincide with the first four terms in the effective Hamiltonian of Refs. [14,15], defined in Eqs. (12)–(15) of the former, with account of the correspondence between the notations used: $E_1 = c_e$, $E_2 = c_I$, $E_3 = b_F$, $E_4 = d_1/[3(2L-1)(2L+3)]$.

The last two terms involving E_5 and E_6, however, do not. The disagreement appears in the terms related to the tensor interaction of the deuterons in the last lines of Eqs. (3) and (5). The explicit expressions for E_4–E_6 are

$$\begin{aligned} E_4 &= \alpha^2 \mu_e \mu_d \frac{m_e}{2m_p}\left[\frac{\langle vL\| r_1^{-5}\big(\mathbf{r}_1^2\delta_{ij} - 3r_{1i}r_{1j}\big)\|vL\rangle}{\langle L\|2\mathbf{L}^2\delta_{ij} - 3(L_iL_j + L_jL_i)\|L\rangle} + (1\to 2)\right], \\ E_5 &= \alpha^2\left(\frac{\mu_d m_e}{2m_p}\right)^2 \frac{\langle vL\| r_{12}^{-5}\big(\delta_{ij}\mathbf{r}_{12}^2 - 3r_{12i}r_{12j}\big)\|vL\rangle}{\langle L\|2\mathbf{L}^2\delta_{ij} - 3(L_iL_j + L_jL_i)\|L\rangle}, \\ E_6 &= Q_d\bar{E}_6,\ \bar{E}_6 = \frac{1}{2}\left[\frac{\langle vL\| r_1^{-5}\big(\delta_{ij}\mathbf{r}_1^2 - 3r_ir_j\big)\|vL\rangle - \langle vL\| r_{12}^{-5}\big(\delta_{ij}\mathbf{r}_{12}^2 - 3r_{12i}r_{12j}\big)\|vL\rangle}{\langle L\|\mathbf{L}^2\delta_{ij} - (3/2)(L_iL_j + L_jL_i)\|L\rangle} + (1\to 2)\right], \end{aligned} \tag{12}$$

where $\langle v'L'\|\ldots\|vL\rangle$ denotes reduced matrix elements in the basis of nonrelativistic wave functions $\psi^{(\mathrm{NR})vLL_z}$, while

$$\langle L\|2\mathbf{L}^2\delta_{ij} - 3(L_iL_j + L_jL_i)\|L\rangle = -2\sqrt{L(L+1)}\sqrt{(2L-1)(2L+1)(2L+3)}$$

is a reduced matrix element in the basis of the representation (L) of $su(2)$ [see Eqs. (7) and (9)].

The point is that the tensor terms in H^{eff} have nonzero matrix elements between "pure" states with even L and different values of the total nuclear spin $I = 0$ and $I' = 2$:

$$\begin{aligned} \langle vLIFJ\|H^{\mathrm{eff}}\|vLI'F'J\rangle &= 10\sqrt{3}(-1)^{J+2F+L+1/2} \\ &\quad\times \sqrt{(2F+1)(2F'+1)}L(L+1)(2L+1)\begin{Bmatrix} F' & F & 2 \\ L & L & J\end{Bmatrix}\begin{Bmatrix} 1 & 1 & 2 \\ L & L & L\end{Bmatrix}\begin{Bmatrix} I & 1/2 & F \\ F' & 2 & I'\end{Bmatrix}(E_5 - E_6), \end{aligned} \tag{13}$$

while the effective Hamiltonian of Refs. [14,15] is *diagonal* in **I**. Neglecting the coupling of pure states with different I affects the values of the hyperfine shifts at the kHz level, as illustrated in Table IV of Sec. II C.

In the first order of perturbation theory, the wave functions of D_2^+ are linear combinations of the basis set (8):

$$\Psi^{(vL)IFJJ_z} = \sum_{I'F'} \beta^{(vL)IFJ}_{I'F'} \Psi_0^{(vL)I'F'JJ_z}, \tag{14}$$

where the constant amplitudes $\beta^{(vL)IFJ}_{I'F'}$ and the hyperfine shifts $\Delta E^{(vL)IFJ}$ are the eigenvectors and eigenvalues of the matrix of $H^{\rm eff}$ in the basis of pure states (9):

$$\sum_{I''F''} H^{{\rm eff}(vL)J}_{I'F',I''F''}\, \beta^{(vL)IFJ}_{I''F''} = \Delta E^{(vL)IFJ} \beta^{(vL)IFJ}_{I'F'}. \tag{15}$$

Similar to H_2^+, symmetry with respect to exchange of the identical nuclei imposes restrictions on the allowed values of I in the summation in Eqs. (14) and (15); for Σ_g states, in particular, I must satisfy $(-1)^{L+I} = 1$. As a result, in H_2^+, in first order of perturbation theory, I turns out to be an exact quantum number [13]. This is not the case for D_2^+, however, where both values $I = 0$ and $I = 2$ are allowed for even values of L, although their mixing is weak. Still, a few of the hyperfine states of D_2^+ are "pure states" with no mixing and all quantum numbers *exact*; these are the states with $I = 1$, $F = 3/2$, $J = L \pm F$ (for odd L), the states with $I = 2$, $F = 5/2$, $J = L \pm F$ (for even $L \geqslant 2$), as well as the states with $L = 0$ and either $I = 0, J = F = 1/2$ or $I = 2, J = F = I \pm 1/2$. The "stretched" states with $F = I + 1/2$, $J = L + F$, and $J_z = \pm J$, of significant experimental interest because their Zeeman shift is strictly linear in the magnetic field in first order of perturbation theory [26], are a subclass of the "pure" states listed above. The hyperfine energy $\Delta E \equiv \Delta E^{(vL)IFJ}$ of the "pure" states is simply expressed in terms of the coefficients of the effective spin Hamiltonian as follows:

$$\Delta E^{(vL)IFJ} = \tfrac{1}{2}[E_3 + L(E_1 + 2E_2 + (2L-1)(E_6 - 2E_4 - 2E_5))], \quad \text{for } I = 1, F = 3/2, J = L + F, \text{ odd } L;$$

$$\Delta E^{(vL)IFJ} = \tfrac{1}{2}[E_3 - (L+1)(E_1 + 2E_2 + (2L+3)(E_6 - 2E_4 - 2E_5))], \quad \text{for } I = 1, F = 3/2, J = L - F, \text{ odd } L \geqslant 3;$$

$$\Delta E^{(vL)IFJ} = E_3 + L(E_1/2 + 2E_2 - (2L-1)(2E_4 + 2E_5 + E_6)), \quad \text{for } I = 2, F = 5/2, J = L + F, \text{ even } L \geqslant 2;$$

$$\Delta E^{(vL)IFJ} = E_3 - (L+1)(E_1/2 + 2E_2 + (2L+3)(2E_4 + 2E_5 + E_6)), \quad \text{for } I = 2, F = 5/2, J = L - F, \text{ even } L \geqslant 4;$$

$$\Delta E^{(v0)0FJ} = 0 \quad \text{for } J = F = 1/2,$$

$$\Delta E^{(v0)2FJ} = -3E_3/2 \quad \text{for } J = F = 3/2,$$

$$\Delta E^{(v0)2FJ} = E_3 \quad \text{for } J = F = 5/2.$$

C. Numerical results

The numerical results of the present work were obtained using the nonrelativistic wave functions $\Psi^{({\rm NR})vLL_z}$ of D_2^+, calculated with high numerical precision in the variational approach of Ref. [27]. Throughout, the calculations the CODATA18 values [8] of fundamental constants were used for m_d/m_p, μ_e, and μ_d, while $Q_d = 0.285783\ {\rm fm}^2$ was taken from Ref. [20].

Table I gives the values of $E_n, n = 1, \ldots, 6$ for the lower rovibrational states of D_2^+; the values for all rovibrational states (vL) with $v \leqslant 10$ and $L \leqslant 4$ can be found in the Supplemental Material [28].

We list the numerical values of $E_n, n = 1, \ldots, 6$ with six significant digits to avoid rounding errors in further calculations, but one should keep in mind that the contribution from QED and relativistic effects of order $O(m_e\alpha^6)$ and higher is not accounted for by the Breit-Pauli Hamiltonian.

We denote by $u(E_n)$ and $u_{\rm r}(E_n)$ the absolute and fractional uncertainties of E_n; $u_{\rm r}(E_n), n \leqslant 5$ are therefore estimated to be order $O(\alpha^2) \approx 0.5 \times 10^{-4}$ [for $u_{\rm r}(E_6)$ see Eq. (16) below]. The numerical uncertainty stemming from numerical integration of the nonrelativistic wave functions $\Psi^{({\rm NR})vLL_z}$ is smaller. Also smaller is the contribution to $u_{\rm r}(E_n)$ from the uncertainty in the values of the physical constants in the Breit-Pauli Hamiltonian (3)–(5), with the important exception of E_6, for which the uncertainty $u(Q_d)$ of the electric quadrupole moment contributes substantially. Indeed, from Eq. (12) we obtain

$$u_{\rm r}(E_6) = \frac{u(E_6)}{E_6} = \sqrt{u_{\rm r}^2(Q_d) + u_{\rm r}^2(\bar{E}_6)} \quad \text{with}$$
$$u_{\rm r}(\bar{E}_6) \sim u_{\rm r}(E_n) \sim O(\alpha^2), \quad n = 1, \ldots, 5. \tag{16}$$

The uncertainty of Q_d arises from uncertainties of both the experimental data and the underlying molecular theory (when Q_d is determined by molecular spectroscopy). The relation between $u_{\rm r}(Q_d)$ and the theoretical uncertainties in the case of D_2^+ spectroscopy is treated in detail in Sec. III D.

The hyperfine energies $\Delta E^{(vL)IFJ}$ and the amplitudes $\beta^{(vL)IFJ}_{I'F'}$ of the states from the hyperfine structure of the lower excited states, calculated using Eqs. (10), (11), and (15), are given in Tables II and III. The results for the higher excited states with v up to 10 or L up to 4 are available in the Supplemental Material [28].

The theoretical uncertainties $u(\Delta E^{(vL)IFJ})$ of the hyperfine energies $\Delta E^{(vL)IFJ}$ were estimated in the assumption that the uncertainties of the coefficients E_n are uncorrelated and are

TABLE I. Numerical values E_n/h, $n = 1, \ldots, 6$, of the coefficients of the effective spin Hamiltonian of Eq. (11) for the lower rovibrational states of D_2^+ with $L \leqslant 4$, $v \leqslant 10$, in MHz. The numbers in brackets denote powers of 10: $a[b] = a \times 10^b$. Note that for $L = 0$ all coefficients but E_3 are zero.

v	L	E_1/h	E_2/h	E_3/h	E_4/h	E_5/h	E_6/h
0	0			142.533			
1	0			139.837			
2	0			137.286			
3	0			134.873			
4	0			132.593			
0	1	21.4599	−3.21518[−3]	142.448	1.32980	−4.71443[−4]	5.67068[−3]
1	1	20.5231	−3.12947[−3]	139.756	1.26978	−4.57403[−4]	5.66924[−3]
2	1	19.6183	−3.04185[−3]	137.209	1.21191	−4.43279[−4]	5.64719[−3]
3	1	18.7423	−2.95244[−3]	134.799	1.15600	−4.29061[−4]	5.60575[−3]
4	1	17.8923	−2.86128[−3]	132.522	1.10187	−4.14738[−4]	5.54600[−3]
0	2	21.3955	−3.20207[−3]	142.278	3.15886[−1]	−1.11799[−4]	1.34038[−3]
1	2	20.4612	−3.11645[−3]	139.594	3.01623[−1]	−1.08462[−4]	1.34003[−3]
2	2	19.5586	−3.02901[−3]	137.054	2.87871[−1]	−1.05106[−4]	1.33480[−3]
3	2	18.6847	−2.93977[−3]	134.652	2.74583[−1]	−1.01728[−4]	1.32498[−3]
4	2	17.8368	−2.84875[−3]	132.382	2.61720[−1]	−9.83254[−5]	1.31082[−3]
0	3	21.2995	−3.18256[−3]	142.025	1.46902[−1]	−5.18607[−5]	6.18729[−4]
1	3	20.3688	−3.09714[−3]	139.353	1.40266[−1]	−5.03083[−5]	6.18561[−4]
2	3	19.4696	−3.00991[−3]	136.824	1.33867[−1]	−4.87468[−5]	6.16135[−4]
3	3	18.5989	−2.92092[−3]	134.432	1.27684[−1]	−4.71753[−5]	6.11585[−4]
4	3	17.7541	−2.83015[−3]	132.173	1.21697[−1]	−4.55926[−5]	6.05027[−4]
0	4	21.1727	−3.15685[−3]	141.691	8.54566[−2]	−3.00678[−5]	3.56385[−4]
1	4	20.2467	−3.07169[−3]	139.033	8.15938[−2]	−2.91641[−5]	3.56285[−4]
2	4	19.3519	−2.98476[−3]	136.519	7.78684[−2]	−2.82552[−5]	3.54880[−4]
3	4	18.4855	−2.89608[−3]	134.142	7.42682[−2]	−2.73407[−5]	3.52246[−4]
4	4	17.6446	−2.80567[−3]	131.896	7.07820[−2]	−2.64197[−5]	3.48452[−4]

given by

$$u(\Delta E^{(vL)IFJ}) = \sqrt{\sum_n \left(u_{\rm r}(E_n)\, \Gamma_n^{(vL)IFJ}\right)^2} \quad \text{with}$$

$$\Gamma_n^{(vL)IFJ} = E_n \frac{\partial \Delta E^{(vL)IFJ}}{\partial E_n}. \tag{17}$$

For states with the smallest shifts ($\simeq$20 MHz, in which the influence of the coefficient E_3 is comparatively small), the uncertainties $u(\Delta E^{(vL)IFJ})$ are of order 1 kHz, while for hyperfine states with shifts of the order of 100 MHz and above the theoretical uncertainty may reach $\approx$10 kHz.

In the lower rovibrational states of D_2^+, the dominating term of the Breit-Pauli Hamiltonian (3)–(5) is the contact spin-spin interaction between the electron and the nuclei; this can be recognized by comparing the value of E_3 with the other coefficients of the effective spin Hamiltonian $H^{\rm eff}$ (11), given in Table I and the Supplemental Material [28].

The contribution to $\Delta E^{(vL)IFJ}$ of the E_3 term alone is $(E_3/2)[F(F+1) - I(I+1) - 3/4]$; similar to H_2^+, it qualitatively determines the shape of the hyperfine level structure (see Fig. 1), and for $L = 0$ this is the only contribution to the hyperfine energy. The typical separation between hyperfine levels of D_2^+ with different values of F or I is of the order of $E_3 \approx 10^2$ MHz. It is significantly smaller than the GHz separation in H_2^+ or HD^+ because of the smaller magnetic dipole moment of the deuteron μ_d as compared with μ_p. For all three molecular ions, the separation between states with $\Delta J = \pm 1$ is of the order of 10 MHz.

The off-diagonal elements of the matrix $\beta_{I'F'}^{IFJ}$ [see Eq. (14)] are small; i.e., the mixing of states with different values of I or F is weak. This justifies our choice of the angular momentum coupling scheme and allows to use in estimates of the characteristics of D_2^+ (except for the hyperfine shifts) the approximation of pure states $\beta_{I'F'}^{IFJ} = \delta_{F'F}\delta_{I'I}$.

Keeping in mind the suggestion by Babb [19] and Zhang *et al.* [14,15] to determine the deuteron electric quadrupole moment Q_d by means of hyperfine spectroscopy of D_2^+, we give in the rightmost column of Tables II and III the (numerically calculated) derivatives of the hyperfine energies with respect to Q_d that describe the sensitivity of $\Delta E^{(vL)IFJ}$ to variations of Q_d. Relevant for the determination of Q_d by direct comparison of the theoretical and experimental values of a specific transition frequency are the differences of the sensitivities of upper and lower state of the transition. (Some of these are given in Table VI.) It can be seen from the largest differences ($\simeq$100 kHz fm^{-2}) that the experimental and theoretical uncertainties have to be on the order of 3 Hz or less, in order to match the present uncertainty of Q_d. Such a small theoretical uncertainty cannot be achieved at present. Therefore, in Sec. III D we discuss an alternative approach to this goal.

The comparison of our results for the hyperfine energies $\Delta E^{(vL)IFJ}$ with earlier calculations is illustrated in Table IV for the $(v = 0, L = 1)$ state taken as representative example.

The difference with the values of Refs. [14,15] is in the kHz range, in agreement with the estimates of the contribution from the off-diagonal matrix elements of the tensor spin interaction terms which were neglected there. The results agree with each other within the estimated theoretical uncertainty

TABLE II. Hyperfine structure of the lower ro-vibrational states for odd values $L = 1, 3$. Listed are: the quantum numbers J, I, and F, the hyperfine energy $\Delta E^{\rm hfs}/h = \Delta E^{(vL)IFJ}/h$ (in MHz), the amplitudes $\beta^{(vL)IFJ}_{I'F'}$ in the expansion (14) of the spin wave function, and the derivative $h^{-1}\, d\Delta E^{\rm hfs}/dQ_d$ (in kHz fm^{-2}). The hyperfine states that are "pure" (listed at the end of Sec. II B), are typed in boldface.

I	F	J	$\Delta E^{\rm hfs}/h$	$\beta^{IFJ}_{1,1/2}$	$\beta^{IFJ}_{1,3/2}$	$(d\Delta E^{\rm hfs}/dQ_d)/h$
			$v = 0, L = 1$			
1	1/2	3/2	−146.999(8)	0.99776	−0.06688	2.78
1	1/2	1/2	−136.493(7)	0.99673	−0.08075	−10.97
1	3/2	1/2	47.916(4)	0.08075	0.99673	60.58
1	3/2	3/2	70.351(4)	0.06688	0.99776	−42.47
1	**3/2**	**5/2**	**80.624(4)**	**0.00000**	**1.00000**	**9.92**
			$v = 1, L = 1$			
1	1/2	3/2	−144.085(7)	0.99787	−0.06524	2.72
1	1/2	1/2	−134.026(7)	0.99692	−0.07838	−10.66
1	3/2	1/2	47.564(4)	0.07838	0.99692	60.25
1	3/2	3/2	69.012(4)	0.06524	0.99787	−42.39
1	**3/2**	**5/2**	**78.870(4)**	**0.00000**	**1.00000**	**9.92**
			$v = 2, L = 1$			
1	1/2	3/2	−141.325(7)	0.99798	−0.06356	2.64
1	1/2	1/2	−131.698(7)	0.99711	−0.07598	−10.30
1	3/2	1/2	47.251(4)	0.07598	0.99711	59.70
1	3/2	3/2	67.746(4)	0.06356	0.99798	−42.16
1	**3/2**	**5/2**	**77.202(4)**	**0.00000**	**1.00000**	**9.88**
			$v = 0, L = 3$			
1	1/2	7/2	−157.925(7)	0.98895	−0.14826	7.53
1	1/2	5/2	−134.446(7)	0.98227	−0.18749	−16.39
1	**3/2**	**3/2**	**23.151(4)**	**0.00000**	**1.00000**	**3.87**
1	3/2	5/2	54.118(3)	0.18749	0.98227	6.65
1	3/2	7/2	80.653(4)	0.14826	0.98895	−40.01
1	**3/2**	**9/2**	**100.754(4)**	**0.00000**	**1.00000**	**16.24**
			$v = 1, L = 3$			
1	1/2	7/2	−154.445(7)	0.98944	−0.14497	7.38
1	1/2	5/2	−131.922(7)	0.98324	−0.18230	−15.94
1	**3/2**	**3/2**	**23.914(4)**	**0.00000**	**1.00000**	**38.96**
1	3/2	5/2	53.336(3)	0.18230	0.98324	6.20
1	3/2	7/2	78.775(4)	0.14497	0.98944	−39.85
1	**3/2**	**9/2**	**98.122(4)**	**0.00000**	**1.00000**	**16.23**
			$v = 2, L = 3$			
1	1/2	7/2	−151.139(7)	0.98992	−0.14161	7.20
1	1/2	5/2	−129.544(7)	0.98421	−0.17702	−15.42
1	**3/2**	**3/2**	**24.678(4)**	**0.00000**	**1.00000**	**38.81**
1	3/2	5/2	52.614(3)	0.17702	0.98421	5.72
1	3/2	7/2	76.992(3)	0.14161	0.98992	−39.54
1	**3/2**	**9/2**	**95.605(4)**	**0.00000**	**1.00000**	**16.17**

because this contribution happens to be numerically of the same order of magnitude.

The difference with Ref. [16] is larger because of the oversimplified form of the tensor spin interactions adopted there. The difference with the experimental values of Ref. [17] for the hyperfine shifts in the same state exceeds by a factor of ≈2 the experimental uncertainty. However, the authors of Ref. [17] themselves do not rule out the possibility that the overall uncertainty reported there is too optimistic.

III. ELECTRIC QUADRUPOLE TRANSITIONS

A. Hyperfine structure of the $E2$ spectra in homonuclear molecular ions

The evaluation of the electric quadrupole transition spectrum of $D_2{}^+$ follows closely the procedure described in details in Ref. [13]; we shall highlight the points that are specific for the $D_2{}^+$ molecule, and also take the opportunity to refine some of the definitions given there. The use of dimensional SI units is restored in the rest of the paper.

Similar to Eqs. (5)–(7) of Ref. [13], we denote by $H^{(E2)}_{\rm int}$ the terms in the interaction Hamiltonian of $D_2{}^+$ with a monochromatic electromagnetic plane wave, which are responsible for the electric quadrupole transitions.

We take the vector potential in the form $\mathbf{A}(\mathbf{R}, t) = (-i/\omega)(\mathbf{E}_0\, e^{i(\mathbf{k}.\mathbf{R}-\omega t)} - \mathbf{E}_0^*\, e^{-i(\mathbf{k}.\mathbf{R}-\omega t)})$, where $\mathbf{k}$ is the wave vector, $\omega = c|\mathbf{k}|$ is the circular frequency, and $\mathbf{E}_0$ is the amplitude of the oscillating electric field,

The $E2$ transition matrix element between the initial $|i\rangle = |(vL)IFJJ_z\rangle$ and final $|f\rangle = |(v'L')I'F'J'J'_z\rangle$ hyperfine states

TABLE III. Hyperfine structure of the lower ro-vibrational states for even values $L=0, 2$. Listed are: the quantum numbers J, I, and F, the hyperfine energy $\Delta E^{\rm hfs}/h = \Delta E^{(vL)IFJ}/h$ (in MHz), the amplitudes $\beta^{(vL)IFJ}_{I'F'}$ in the expansion (14) of the spin wave function, and the derivative $h^{-1}\, d\Delta E^{\rm hfs}/dQ_d$ (in kHz fm^{-2}). The hyperfine states that are "pure" (listed at the end of Sec. II B), are typed in boldface. Note that the values of $\beta^{IFJ}_{0,1/2}$, $I=0$, $F=1/2$, $L=2$ are strictly less than 1 but appear as 1.00000 due to rounding to 5 significant digits. On the contrary, $\Delta E^{\rm hfs}$ for $I=0$, $F=J=1/2$ is strictly zero.

I	F	J	$\Delta E^{\rm hfs}/h$	$\beta^{IFJ}_{0,1/2}$	$\beta^{IFJ}_{2,3/2}$	$\beta^{IFJ}_{2,5/2}$	$(d\Delta E^{\rm hfs}/dQ_d)/h$
				$v=0, L=0$			
2	**3/2**	**3/2**	**−213.800(11)**	**0.00000**	**1.00000**	**0.00000**	**0.00000**
0	**1/2**	**1/2**	**0.000(8)**	**1.00000**	**0.00000**	**0.00000**	**0.00000**
2	**5/2**	**5/2**	**142.533(8)**	**0.00000**	**0.00000**	**1.00000**	**0.00000**
				$v=1, L=0$			
2	**3/2**	**3/2**	**−209.756(11)**	**0.00000**	**1.00000**	**0.00000**	**0.00000**
0	**1/2**	**1/2**	**0.000(0)**	**1.00000**	**0.00000**	**0.00000**	**0.00000**
2	**5/2**	**5/2**	**139.837(7)**	**0.00000**	**0.00000**	**1.00000**	**0.00000**
				$v=0, L=2$			
2	3/2	7/2	−226.255(11)	0.00000	0.99852	−0.05446	−22.25
2	3/2	5/2	−216.433(11)	0.00004	0.99669	−0.08128	51.39
2	3/2	3/2	−202.716(11)	−0.00012	0.99664	−0.08194	5.06
2	3/2	1/2	−190.986(11)	0.00000	0.99863	−0.05238	−66.45
0	1/2	3/2	−32.093(2)	1.00000	0.00012	0.00006	0.01
0	1/2	5/2	21.395(1)	1.00000	−0.00002	0.00019	−0.02
2	5/2	1/2	102.515(8)	0.00000	0.05238	0.99863	−81.29
2	5/2	3/2	117.107(7)	−0.00007	0.08194	0.99664	−33.21
2	5/2	5/2	135.572(7)	−0.00019	0.08128	0.99669	26.03
2	5/2	7/2	151.994(7)	0.00000	0.05446	0.99852	50.39
2	**5/2**	**9/2**	**159.864(8)**	**0.00000**	**0.00000**	**1.00000**	**−28.14**
				$v=1, L=2$			
2	3/2	7/2	−221.646(11)	0.00000	0.99858	−0.05318	−22.19
2	3/2	5/2	−212.213(11)	0.00004	0.99686	−0.07921	51.32
2	3/2	3/2	−199.097(11)	−0.00012	0.99682	−0.07963	4.92
2	3/2	1/2	−187.921(11)	0.00000	0.99871	−0.05076	−66.51
0	1/2	3/2	−30.692(2)	1.00000	0.00013	0.00007	0.01
0	1/2	5/2	20.461(1)	1.00000	−0.00002	0.00019	−0.02
2	5/2	1/2	101.558(8)	0.00000	0.05076	0.99871	−81.19
2	5/2	3/2	115.469(7)	−0.00008	0.07963	0.99682	−33.07
2	5/2	5/2	133.118(7)	−0.00019	0.07921	0.99686	26.07
2	5/2	7/2	148.851(7)	0.00000	0.05318	0.99858	50.33
2	**5/2**	**9/2**	**156.416(7)**	**0.00000**	**0.00000**	**1.00000**	**−28.13**
				$v=2, L=2$			
2	3/2	7/2	−217.273(11)	0.00000	0.99865	−0.05189	−22.05
2	3/2	5/2	−208.218(11)	0.00004	0.99702	−0.07710	51.07
2	3/2	3/2	−195.684(11)	−0.00012	0.99701	−0.07728	4.76
2	3/2	1/2	−185.041(11)	0.00000	0.99879	−0.04913	−6.63
0	1/2	3/2	−29.338(2)	1.00000	0.00013	0.00007	0.01
0	1/2	5/2	19.559(1)	1.00000	−0.00002	0.00019	−0.02
2	5/2	1/2	100.687(7)	0.00000	0.04913	0.99879	80.80
2	5/2	3/2	113.941(7)	−0.00008	0.07728	0.99701	−32.80
2	5/2	5/2	130.803(7)	−0.00019	0.07710	0.99702	26.02
2	5/2	7/2	145.870(7)	0.00000	0.05189	0.99865	50.07
2	**5/2**	**9/2**	**153.139(7)**	**0.00000**	**0.00000**	**1.00000**	**−28.02**

of $D_2{}^+$ is

$$\langle \Psi^{(v'L')I'F'J'J'_z} | H^{(E2)}_{\rm int} | \Psi^{(vL)IFJJ_z} \rangle = \frac{i}{3c}\, \omega^{\rm NR}\, |\mathbf{E}_0| \big(e^{-i\omega t} \langle \Psi^{(v'L')I'F'J'J'_z} |\, \widehat{T}^{(2)}_{ij}\, Q^{(2)}_{ij}\, | \Psi^{(vL)IFJJ_z} \rangle + e^{i\omega t} \langle \Psi^{(v'L')I'F'J'J'_z} |\, \widehat{T}^{(2)*}_{ij}\, Q^{(2)}_{ij}\, | \Psi^{(vL)IFJJ_z} \rangle \big), \tag{18}$$

where $\omega^{\rm NR} = (E^{({\rm NR})v'L'} - E^{({\rm NR})vL})/\hbar$ is the transition circular frequency in the nonrelativistic approximation, the asterisk denotes complex conjugation, and the tensor of the electric quadrupole transition operator is defined as

$$Q^{(2)}_{ij} = \frac{1}{2} \sum_\alpha Z_\alpha e \big(3 R_{\alpha i} R_{\alpha j} - \delta_{ij}\, \mathbf{R}^2_\alpha \big), \tag{19}$$

where the summation here is over the constituents of $D_2{}^+$ ($\alpha = 1, 2$ referring to nuclei 1 and 2 and $\alpha = 3$ labeling the electron) and $Z_\alpha e$ is the corresponding electric charge. $\widehat{T}^{(2)}$ is

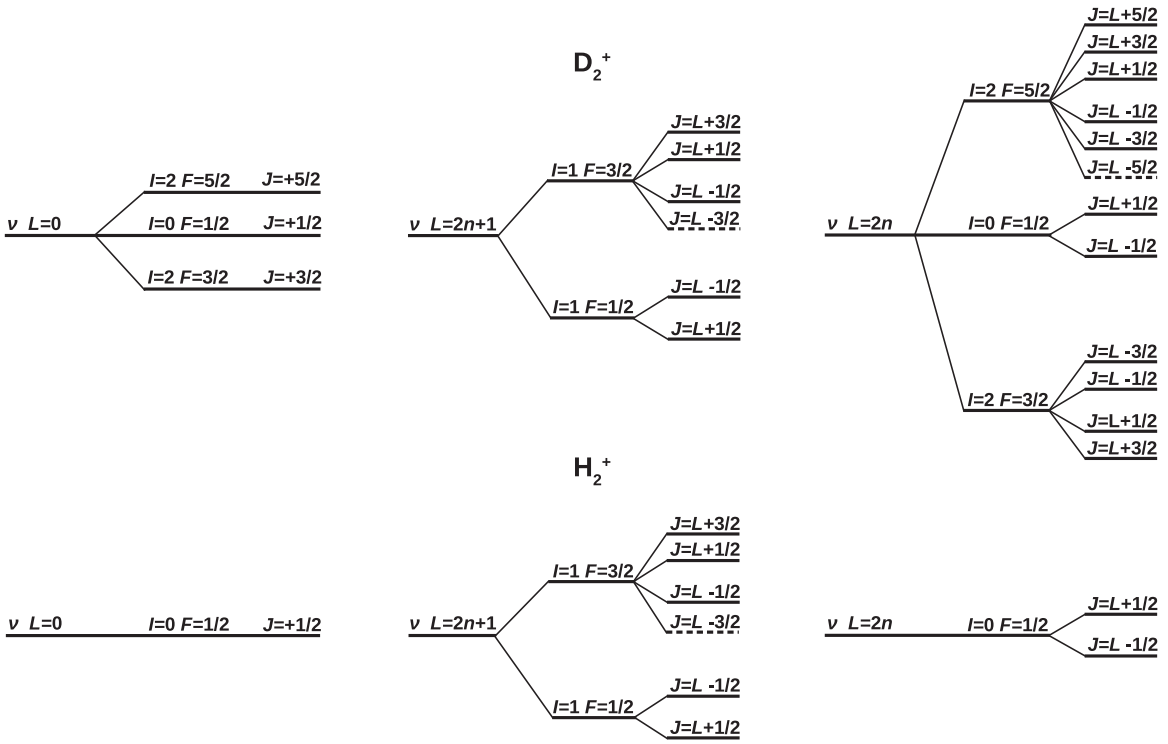

FIG. 1. Comparison of the hyperfine structure of the molecular ions $D_2{}^+$ and $H_2{}^+$, for even $L = 2n$, $n = 1, 2, \ldots$ and odd $L = 2n + 1$, $n = 0, 1, \ldots$ values of L and for $L=0$. For $1 \leqslant L \leqslant 2$, the states marked with dashed lines do not exist (see Tables II and III). For $L=0$, the HFS of $D_2{}^+$ consists of only three states; like $H_2{}^+$, the one with $I=0$ has no hyperfine shift.

a tensor of rank 2 with Cartesian components

$$\widehat{T}^{(2)}_{ij} = \tfrac{1}{2}(\hat{k}_i\hat{\epsilon}_j + \hat{k}_j\hat{\epsilon}_i), \quad \hat{\mathbf{k}}\cdot\hat{\boldsymbol{\epsilon}} = 0, \tag{20}$$

where $\hat{\mathbf{k}} = \mathbf{k}/|\mathbf{k}|$ and $\hat{\boldsymbol{\epsilon}}$ is a unit vector of polarization, $\mathbf{E}_0 = \hat{\boldsymbol{\epsilon}}\,|\mathbf{E}_0|$. Einstein's convention for summation over repeated pairs of indices of Cartesian components of vectors and tensors is assumed in Eq. (18) and further on.

To switch from Cartesian to cyclic coordinates and back for the symmetric tensor operators of rank 2, we use a convention, $Q^{(2)}_0 = Q^{(2)}_{zz}$, that implies

$$T^{(2)}_{ij}Q^{(2)}_{ij} = \frac{3}{2}\sum_q (-1)^q T^{(2)}_q Q^{(2)}_{-q} = \frac{3}{2}(T^{(2)}\cdot Q^{(2)}).$$

Note that, in a general case of elliptic polarization, the vector $\hat{\boldsymbol{\epsilon}}$ and tensor $\widehat{T}^{(2)}$ are complex.

TABLE IV. Comparison of the numerical values of the hyperfine energies $\Delta E^{(vl)IFJ}/h$ for the $(vL) = (01)$ state, in MHz, calculated in the present work and in Refs. [14,16].

I	F	J	This work	[14]	[16]
			$(vL) = (01)$		
1	3/2	5/2	80.624(4)	80.623(4)	80.597
1	3/2	3/2	70.351(4)	70.355(4)	70.319
1	3/2	1/2	47.916(4)	47.910(3)	47.878
1	1/2	1/2	−136.493(7)	−136.492(7)	−136.436
1	1/2	3/2	−146.999(8)	−146.999(8)	−146.94

The matrix elements of the scalar product $\widehat{T}^{(2)}\cdot Q^{(2)}$ in Eq. (18) have the form

$$\begin{aligned}\langle\Psi^{(v'L')I'F'J'J'_z}|\widehat{T}^{(2)}_{ij}Q^{(2)}_{ij}|\Psi^{(vL)IFJJ_z}\rangle \\ = \frac{3}{2}\sqrt{2J+1}\sum_q \widehat{T}^{(2)q}\,C^{J'J'_z}_{JJ_z,2q}\Bigg[\sum_{I_1F_1}(-1)^{J+L+F_1} \\ \times\begin{Bmatrix} L & F_1 & J \\ J' & 2 & L'\end{Bmatrix}\beta^{(vL)IFJ}_{I_1F_1}\beta^{(v'L')I'F'J'}_{I_1F_1}\Bigg]\langle v'L'\|Q^{(2)}\|vL\rangle, \\ q = J'_z - J_z,\end{aligned} \tag{21}$$

and similarly for the conjugate one, where $\langle v'L'\|Q^{(2)}\|vL\rangle$ are the reduced matrix elements of $Q^{(2)}$. The Rabi frequency for the transition $|i\rangle \to |f\rangle$ is expressed in terms of these matrix elements as follows:

$$\Omega_{if} = \frac{\omega_{if}\,|\mathbf{E}_0|}{3\hbar c}\langle\Psi^{(v'L')I'F'J'J'_z}|\widehat{T}^{(2)}_{ij}Q^{(2)}_{ij}|\Psi^{(vL)IFJJ_z}\rangle, \tag{22}$$

where $\omega_{if} = (E^{(v'L')I'F'J'} - E^{(vL)IFJ})/\hbar$. Note that for general polarization Ω_{if} is complex.

The probability per unit time $\mathcal{W}_{if}$ for the transition $|i\rangle \to |f\rangle$, stimulated by the external electric field with amplitude $\mathbf{E}_0$, oscillating with frequency ω and propagating along $\mathbf{k}$, may be expressed in terms of the Rabi frequency as follows: $\mathcal{W}_{if} = 2\pi(\delta(\omega-\omega_{if}) + \delta(\omega+\omega_{if}))|\Omega_{if}|^2$. We shall put it in the factorized form used in Eq. (18) of Ref. [13]:

$$\begin{aligned}\mathcal{W}_{if} = &\mathcal{W}^{\rm NR}(v'L';vL)\,\mathcal{W}^{\rm hfs}((v'L')I'F'J';\\ &(vL)IFJ)\,\mathcal{W}^{\rm pol}(J'J'_z;J_z).\end{aligned} \tag{23}$$

The first factor, $\mathcal{W}^{\rm NR}(v'L';vL)$, is the rate of stimulated $E2$ transitions in $D_2{}^+$ in the nonrelativistic (spinless) approximation, averaged over the initial and summed over the final angular momentum projections L_z, L'_z,

$$\mathcal{W}^{\rm NR}(v'L';vL) = \frac{\pi\omega_{if}^2}{\varepsilon_0 c^3\hbar^2}\frac{1}{15(2L+1)}|\langle v'L'\|Q^{(2)}\|vL\rangle|^2\,\bar{\mathcal{I}},$$
$$\bar{\mathcal{I}} = \int d\omega\,\mathcal{I}(\omega)g_{if}(\omega), \tag{24}$$

where $\mathcal{I}(\omega)$ is the spectral density of the external (laser) field energy flux, and $g_{if}(\omega)$ is the transition line spectral profile.

The factor

$$\mathcal{W}^{\rm hfs}((v'L')I'F'J';(vL)IFJ) = (2L+1)(2J'+1) \times\left(\sum_{I_1F_1}\beta^{(v'L')I'F'J'}_{I_1F_1}\beta^{(vL)IFJ}_{I_1F_1}(-1)^{J+F_1}\begin{Bmatrix}L & F_1 & J\\ J' & 2 & L'\end{Bmatrix}\right)^2, \tag{25}$$

describes the intensity of the individual hyperfine component $IFJ\to I'F'J'$ of the transition line $(vL)\to(v'L')$.

Because of the weak mixing of the pure states in Eq. (14) (see Tables II and III), a good approximation for the intensity of the strong (favored) transitions is to assume that $\beta^{(vL)IFJ}_{I'F'}\approx\delta_{I'I}\delta_{F'F}$ that leads to

$$\mathcal{W}^{\rm hfs}((v'L')IFJ';(vL)IFJ) \approx (2L+1)(2J'+1)\begin{Bmatrix}L & F & J\\ J' & 2 & L'\end{Bmatrix}^2. \tag{26}$$

The weak (unfavored) transitions are forbidden in this approximation.

Finally,

$$\mathcal{W}^{\rm pol}(J'J'_z;JJ_z) = \frac{15(2J+1)}{2J'+1}\left(C^{J'J'_z}_{JJ_z,2q}\right)^2|\widehat{T}^{(2)}_q|^2,$$
$$q = J'_z - J_z, \tag{27}$$

is related to the intensity of the Zeeman components of a hyperfine transition line with different values of the magnetic quantum numbers J_z, J'_z. $\mathcal{W}^{\rm pol}(J'J'_z;JJ_z)$ is normalized with the condition

$$\frac{1}{2J+1}\sum_{J_z;J'_z}\mathcal{W}^{\rm pol}(J'J'_z,JJ_z) = 1. \tag{28}$$

Note that compared with Eqs. (20) and (21) of Ref. [13], the factor $(2J+1)$ has now been moved from $\mathcal{W}^{\rm hfs}$ to $\mathcal{W}^{\rm pol}$. In the absence of an external magnetic field or in the case of spectral resolution insufficient to distinguish the Zeeman components, the rate $\mathcal{W}_1$ of excitation of an individual hyperfine component J_z to any of the Zeeman states J'_z is independent of J_z, and using Eqs. (23) and (28) it is reduced to $\mathcal{W}_1 = \mathcal{W}^{\rm NR}(v'L';vL)\,\mathcal{W}^{\rm hfs}((v'L')I'F'J';(vL)IFJ)$. Similarly, the product $\mathcal{W}^{\rm hfs}((v'L')I'F'J';(vL)IFJ)\,\mathcal{W}^{\rm pol}(J'J'_z;JJ_z)$ satisfies the normalization condition

$$\sum_{I'F'J'J'_z}\frac{1}{n^{\rm hfs}(vL)}\sum_{IFJJ_z}\mathcal{W}^{\rm hfs}((v'L')I'F'J';(vL)IFJ) \times\mathcal{W}^{\rm pol}(J'J'_z;JJ_z) = 1, \tag{29}$$

where the sum is over the allowed values of I, I' with the same parity as L, and $n^{\rm hfs}(vL)$ is the number of states in the considered hyperfine manifold of the (vL) state:

$$n^{\rm hfs}(vL) = \begin{cases}6(2L+1) & \text{for odd } L,\\ 12(2L+1) & \text{for even } L.\end{cases} \tag{30}$$

In case the hyperfine structure of the $E2$ transition line is not resolved, the excitation rate $\mathcal{W}_2$ from any of the $n^{\rm hfs}(vL)$ initial states to all final states is found by summing $\mathcal{W}_{if}$ of Eq. (23) over all final states and averaging over all initial states. The result is $\mathcal{W}_2 = \mathcal{W}^{\rm NR}(v'L';vL)$.

B. Laser polarization effects on the Zeeman structure of $E2$ spectra

Recent progress in the precision spectroscopy of the HD^+ molecular ion [6] has made it possible to resolve the Zeeman structure of laser-induced $E1$ transition lines. This allowed us to quantitatively study the Zeeman and Stark shifts of the spectral lines, to reduce the related systematic uncertainties, and to determine the electron-to-proton mass ratio with improved accuracy.

Anticipating the future precision spectroscopy of the $D_2{}^+$ ion, we consider here some general characteristics of the Zeeman structure of laser-induced electric quadrupole transitions and reveal effects of the polarization of the stimulating laser light that appear only in higher multipolarity spectra. These effects are described by the factor $\mathcal{W}^{\rm pol}(J'J'_z;JJ_z)$ in Eq. (23) and impact the intensity but not the frequency of the $E2$ transition lines; the calculations of the Zeeman shift of the transition frequencies will be published elsewhere.

The cyclic components of the rank-2 irreducible tensor $\widehat{T}^{(2)}$ (20) are expressed in terms of the Cartesian components as follows:

$$\widehat{T}^{(2)\pm2} = \sqrt{\frac{1}{6}}[\hat{k}_x\hat{\epsilon}_x - \hat{k}_y\hat{\epsilon}_y \mp i(\hat{k}_x\hat{\epsilon}_y + \hat{k}_y\hat{\epsilon}_x)],$$
$$\widehat{T}^{(2)\pm1} = \sqrt{\frac{1}{6}}[\mp(\hat{k}_x\hat{\epsilon}_z + \hat{k}_z\hat{\epsilon}_x) + i(\hat{k}_z\hat{\epsilon}_y + \hat{k}_y\hat{\epsilon}_z)],$$
$$\widehat{T}^{(2)0} = \frac{1}{3}(2\hat{k}_z\hat{\epsilon}_z - \hat{k}_x\hat{\epsilon}_x - \hat{k}_y\hat{\epsilon}_y) = \hat{k}_z\hat{\epsilon}_z. \tag{31}$$

We have updated the normalization of these components as compared with Ref. [13], but have kept unchanged the parametrization of the complex unit vector $\hat{\boldsymbol{\epsilon}} = \mathbf{E}_0/|\mathbf{E}_0|$ pointing along the electric field amplitude $\mathbf{E}_0$.

As in Ref. [13], we denote by K the laboratory reference frame with z axis along the external magnetic field $\mathbf{B}$, by K' a reference frame with z axis along $\hat{\mathbf{k}}$, and take the Cartesian coordinates $(\epsilon'_x, \epsilon'_y, \epsilon'_z)$ of $\hat{\boldsymbol{\epsilon}}$ in K' to be $(\cos\theta, \sin\theta\, e^{i\varphi}, 0)$.

Linear polarization of the incident light is described by $\varphi = 0$ and left-right circular polarization by $\varphi = \pm\pi/2, \theta = \pi/4$; all other combinations correspond to general elliptic polarization. Let (α, β, γ) be the Euler angles of the rotation that transforms K into K', and denote by $M(\alpha, \beta, \gamma)$

the matrix relating the Cartesian coordinates (a_x, a_y, a_z) and (a'_x, a'_y, a'_z) of an arbitrary vector **a** in K and K', respectively: $a_i = \sum_j M_{ij}(\alpha, \beta, \gamma)\, a'_j$. (To avoid mismatch of M with M^{-1}, note that, e.g., $M_{xz} = -\sin\beta\, \cos\gamma$.) In this way, the absolute values of the components of $\widehat{T}$ in the laboratory frame K, appearing in Eq. (27), are parametrized with the *four* angles α, β, θ, and φ (the dependence on γ being canceled):

$$
\begin{aligned}
|\widehat{T}^{(2)\pm 2}|^2 &= -\tfrac{1}{12}\sin^4\beta(1+\cos 2\alpha\cos 2\theta+\sin 2\alpha\sin 2\theta\cos\varphi)\\
&\quad +\tfrac{1}{6}\sin^2\beta(1\pm\cos\beta\ \sin 2\theta\ \sin\varphi),\\
|\widehat{T}^{(2)\pm 1}|^2 &= \tfrac{1}{12}+\tfrac{1}{24}\cos 2\beta\,(1-\cos 2\alpha\ \cos 2\theta)\\
&\quad +\tfrac{1}{24}\cos 4\beta\,(1+\cos 2\alpha\ \cos 2\theta)\\
&\quad -\tfrac{1}{12}(1+2\cos 2\beta)\sin^2\beta\ \sin 2\alpha\ \sin 2\theta\ \cos\varphi\\
&\quad \pm\tfrac{1}{6}\cos\beta\ \cos 2\beta\ \sin 2\theta\ \sin\varphi,\\
|\widehat{T}^{(2)0}|^2 &= \tfrac{1}{8}\sin^2 2\beta\,(1+\cos 2\alpha\cos 2\theta+\sin 2\alpha\sin 2\theta\cos\varphi).
\end{aligned}
\tag{32}
$$

This leads, for linear polarization ($\varphi = 0$), to

$$
\begin{aligned}
\left|\widehat{T}^{(2)\pm 2}_{\rm lin}\right|^2 &= \tfrac{1}{6}\sin^2\beta\,[1-\sin^2\beta\ \cos^2(\theta-\alpha)],\\
\left|\widehat{T}^{(2)\pm 1}_{\rm lin}\right|^2 &= \tfrac{1}{12}\,[1+\cos 4\beta\cos^2(\theta-\alpha)+\cos 2\beta\sin^2(\theta-\alpha)],\\
\left|\widehat{T}^{(2)0}_{\rm lin}\right|^2 &= \tfrac{1}{4}\sin^2 2\beta\cos^2(\theta-\alpha),
\end{aligned}
\tag{33}
$$

and for left circular polarization ($\theta = \pi/4, \varphi = \pi/2$)

$$
\begin{aligned}
\left|\widehat{T}^{(2)\pm 2}_{\rm left}\right|^2 &= \frac{1}{3}\sin^2\beta\begin{pmatrix}\cos^4\frac{\beta}{2}\\ \sin^4\frac{\beta}{2}\end{pmatrix},\\
\left|\widehat{T}^{(2)\pm 1}_{\rm left}\right|^2 &= \frac{1}{3}\,(1\mp 2\cos\beta)^2\begin{pmatrix}\cos^4\frac{\beta}{2}\\ \sin^4\frac{\beta}{2}\end{pmatrix},\\
\left|\widehat{T}^{(2)0}_{\rm left}\right|^2 &= \frac{1}{8}\sin^2 2\beta.
\end{aligned}
\tag{34}
$$

For right circular polarization, described by $\theta = \pi/4$, $\varphi = -\pi/2$, the values of $|\widehat{T}^{(2)q}_{\rm right}|^2$ are obtained from the above expressions with the substitution $|\widehat{T}^{(2)q}_{\rm right}|^2 = |\widehat{T}^{(2)-q}_{\rm left}|^2$.

One might expect the intensity of the Zeeman components of the $E2$-transition spectrum to depend—as in $E1$ transitions—on three parameters only: one related to the laser polarization and two more describing the mutual orientation of the external magnetic field **B** and the unit vectors $\hat{\mathbf{k}}$ and $\hat{\boldsymbol{\epsilon}}$. In fact, Eqs. (33) and (34) show that this is the case for circular and linear polarization only (when the difference $\theta - \alpha$ appears as a single parameter) while in the general case $\mathcal{W}^{\rm pol}(J'J'_z; JJ_z)$ depends substantially on both angles α and θ. As an illustration, on Fig. 2 are plotted the relative intensities of the Zeeman components $|(vL)IFJ, J_z\rangle = |(00)0\tfrac{1}{2}\tfrac{1}{2}, \tfrac{1}{2}\rangle \to |(12)0\tfrac{1}{2}\tfrac{3}{2}, \tfrac{1}{2}+\Delta\rangle$, $\Delta = -2, -1, 0, 1$ as functions of α for the randomly selected values $\beta = 72^\circ, \theta = 56^\circ, \varphi = 51^\circ$. The plot shows that the measurement of one or other individual Zeeman component of $E2$ transition lines may be substantially enhanced with appropriate optimization of the setup geometry using Eqs. (32)–(34).

The rather sharp dependence of the intensity of the individual Zeeman components on $\theta - \alpha$ for linear polarization and fixed value of the angle β between **B** and the laser propagation direction [cf. Eq. (33)] is shown in Fig. 3.

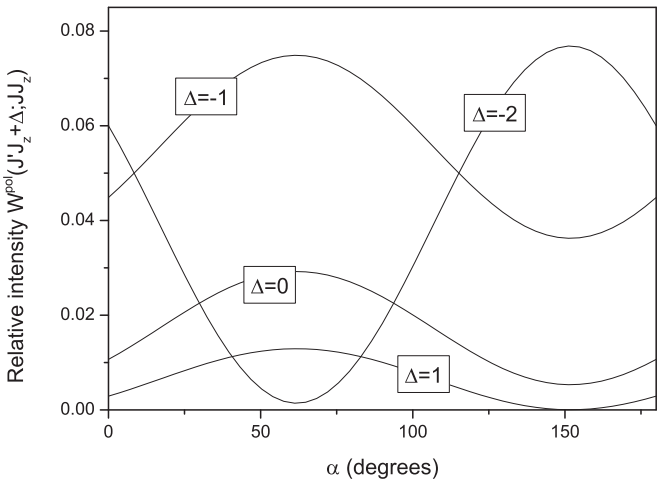

FIG. 2. Relative intensities $\mathcal{W}^{\rm pol}(J'J'_z; JJ_z)$ of the Zeeman components $(JJ_z) = (\tfrac{1}{2}\tfrac{1}{2}) \to (J'J'_z) = (\tfrac{3}{2}\tfrac{1}{2}+\Delta)$, $\Delta = -2, \ldots, 1$ as function of α for randomly selected fixed values of the angles $\beta = 72^\circ, \theta = 56^\circ, \varphi = 51^\circ$ [cf. Eq. (32)].

C. Numerical results

The rate $\mathcal{W}^{\rm NR}(v'L'; vL)$ of laser stimulated $E2$ transitions between the rovibrational states $|vL\rangle$ and $|v'L'\rangle$ of the molecular ion $D_2{}^+$ are expressed in Eq. (24) in terms of the reduced matrix elements $\langle v'L'\|Q^{(2)}\|vL\rangle$ of the electric quadrupole moment of $D_2{}^+$ between these states. In the present work, the reduced matrix elements were evaluated using the nonrelativistic wave functions of $D_2{}^+$ calculated in the variational approach of Ref. [27]. The numerical values needed for the evaluation of the rate of $E2$ transitions between a few selected rovibrational states are given in Table V. For these transitions, the table also lists the values of the Einstein's coefficients

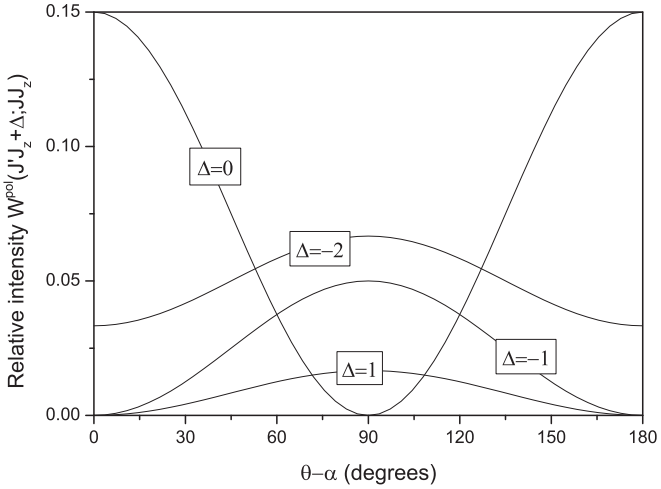

FIG. 3. Relative intensities $\mathcal{W}^{\rm pol}(J'J'_z; JJ_z)$ of the Zeeman components $(JJ_z) = (\tfrac{1}{2}\tfrac{1}{2}) \to (J'J'_z) = (\tfrac{3}{2}\tfrac{1}{2}+\Delta)$, $\Delta = -2, \ldots, 1$, stimulated with linearly polarized laser light, as function of $\theta - \alpha$ for $\beta = 45^\circ$ [cf. Eq. (33)].

TABLE V. Numerical values of the nonrelativistic energies $\Delta E^{\rm NR}/hc = (E^{({\rm NR})v'L'} - E^{({\rm NR})vL})/hc$ (in cm^{-1}), of the reduced matrix elements $|\langle v'L'||Q^{(2)}||vL\rangle|/ea_0^2$ of the deuteron electrical quadrupole moment defined in Eq. (19), and of the Einstein coefficients $A_{v'L'\to vL}$ (in s^{-}1) for selected $E2$ transitions between the rovibrational states $|vL\rangle$ and $|v'L'\rangle$ of D_2^+. For comparison, the results of Pilon [12] are also given when available. $a[b]$ stands for $a \times 10^b$.

				$A_{v'L'\to vL}$ (s^{-1})	
(vL)	$(v'L')$	$\Delta E^{\rm NR}/hc$ (cm^{-1})	$\lvert\langle v'L'\lVert Q^{(2)}\rVert vL\rangle\rvert/ea_0^2$	This work	Olivares-Pilón [12]
(00)	(02)	88.053	1.608226	0.30665[−12]	0.30665[−12]
(00)	(12)	1661.833	0.267274	0.20281[−07]	0.20281[−07]
(00)	(22)	3171.009	0.019403	0.27036[−08]	0.27036[−08]
(00)	(32)	4617.211	0.002497	0.29299[−09]	0.29298[−09]
(00)	(42)	6001.881	0.000451	0.35543[−10]	
(00)	(62)	8591.673	0.000027	0.77727[−12]	
(01)	(11)	1575.973	0.311496	0.35215[−07]	0.35215[−07]
(01)	(21)	3087.284	0.019765	0.40905[−08]	0.40905[−08]
(01)	(31)	4535.575	0.002284	0.37384[−09]	0.37382[−09]
(01)	(41)	5922.282	0.000367	0.36679[−10]	
(02)	(12)	1573.782	0.340448	0.25064[−07]	0.25064[−07]
(02)	(22)	3082.958	0.021629	0.29183[−08]	0.29182[−08]
(02)	(42)	5913.830	0.000403	0.26277[−10]	
(03)	(11)	1429.607	0.420823	0.39479[−07]	0.39479[−07]
(04)	(12)	1369.684	0.522608	0.29490[−07]	
(04)	(24)	3067.885	0.027948	0.26415[−08]	
(04)	(32)	4325.062	0.001717	0.99945[−10]	0.99939[−10]
(06)	(56)	7145.142	0.000129	0.26793[−11]	
(11)	(13)	140.894	2.379256	0.50287[−11]	0.50287[−11]
(11)	(33)	3089.955	0.048979	0.10811[−07]	0.10811[−07]
(20)	(42)	2912.431	0.052069	0.12725[−07]	
(32)	(64)	4135.286	0.024586	0.90959[−08]	
(52)	(54)	167.679	4.033412	0.26834[−10]	

$A_{v'L'\to vL}$, which are related to the reduced matrix elements by

$$A_{v'L'\to vL}/t_0^{-1} = \frac{\alpha^5}{15(2L+1)}[(E^{{\rm NR}v'L'} - E^{{\rm NR}vL})/\mathcal{E}_0]^5 \left(\langle v'L'\|Q^{(2)}\|vL\rangle/ea_0^2\right)^2, \quad (35)$$

where a_0, $t_0 = a_0/\alpha c$, and $\mathcal{E}_0 = 2{\rm Ry}$ are the atomic units of length, time, and energy. The comparison with the values calculated by Pilon [12] with different methods for a partly overlapping selection of transitions shows good agreement for the lower excited states, and indications of possible discrepancy of the order of 10^{-4} for the higher vibrational excitations.

Juxtaposition with the analogous Table II of Ref. [13] shows that the rates of spontaneous transitions in D_2^+ are suppressed in comparison with H_2^+. This is mainly due to the smaller rotational and vibrational excitation energies, related to the larger nuclear mass. In addition to Table V, the Supplemental Material [28] gives the list of the reduced matrix elements for all $E2$ transitions between the rovibrational states with $v \leqslant 10$ and $L \leqslant 4$.

Further on, using the values of the amplitudes $\beta_{I'F'}^{(vL)IFJ}$, obtained by diagonalization of the effective spin Hamiltonian matrix (15), we calculated the coefficients $\mathcal{W}^{\rm hfs}((v'L')I'F'J';(vL)IFJ)$, in the expression (23) for the rate of the individual hyperfine components. Figure 4 illustrates the hyperfine structure of the $E2$ transition $|01\rangle \to |11\rangle$ and is representative also for other rovibrational transitions.

The spectrum consists of "strong" (favored) components between hyperfine states with the same values of the quantum numbers F and I spread over a range up to ±50 MHz around the center of gravity of the hyperfine manifold, and "weak" components between states with $\Delta F \neq 0$ or $\Delta I \neq 0$ at a distance of a few hundred MHz. The weak components are suppressed due to the relatively weak mixing of F and I in the eigenstates of the effective spin Hamiltonian matrix. Compared to H_2^+, however, the suppression in D_2^+ is less pronounced; the reason is that because of the smaller nuclear magnetic moment of the deuteron, the contact spin-spin interactions dominate to a lesser extent, thus leaving room for more F and I mixing.

Table VI lists the details of the "strong" (favored) hyperfine components of four selected $E2$ transition lines: one rotational transition, two fundamental vibrational transitions, and one vibrational overtone transition.

The Supplemental Material [28] includes a table of the hyperfine structure of all $E2$ transition lines between the rovibrational states with $v \leqslant 10$ and $L \leqslant 4$.

D. Determining Q_d by the composite frequency method

The currently available most accurate values of the deuteron electric quadrupole moment Q_d have been obtained by combining the experimental results about the tensor interaction constant (traditionally denoted by d) in the $L = 1$ state of the molecule D_2 from Ref. [29] with the high-precision

TABLE VI. The hyperfine shifts $\Delta E^{\rm hfs}/h = (\Delta E^{(v'L')IFJ'} - \Delta E^{(vL)IFJ})/h$, in MHz, the relative intensities $\mathcal{W}^{\rm hfs} = \mathcal{W}^{\rm hfs}((v'L')IFJ';(vL)IFJ)$, defined in Eq. (25), and the derivative $(d\Delta E^{\rm hfs}/dQ_d)/h$ for the "strong" (favored) components in the hyperfine spectrum of two $E2$ transitions in D_2^+. The transitions between the stretched states, defined in Sec. II B, are shown in boldface.

i	I	F	J	J'	$\Delta E^{\rm hfs}/h$ (MHz)	$\mathcal{W}^{\rm hfs}$	$(d\Delta E^{\rm hfs}/dQ_d)/h$ (kHz fm^{-2})
			$(vL) = (00) \to (v'L') = (02)$				
1	2	5/2	5/2	1/2	−40.018(11)	0.06648	−81.29
2	0	1/2	1/2	3/2	−32.093(2)	0.40000	0.01
3	2	5/2	5/2	3/2	−25.426(11)	0.13244	−33.21
4	2	3/2	3/2	7/2	−12.456(16)	0.39882	−22.25
5	2	5/2	5/2	5/2	−6.961(11)	0.19868	26.03
6	2	3/2	3/2	5/2	−2.633(16)	0.29802	51.39
7	2	5/2	5/2	7/2	9.461(11)	0.26588	50.39
8	2	3/2	3/2	3/2	11.084(16)	0.19866	5.06
9	**2**	**5/2**	**5/2**	**9/2**	**17.331(11)**	**0.33333**	**−28.14**
10	**0**	**1/2**	**1/2**	**5/2**	**21.395(1)**	**0.60000**	**−0.02**
11	2	3/2	3/2	1/2	22.814(16)	0.09973	−66.45
			$(vL) = (00) \to (v'L') = (12)$				
1	2	5/2	5/2	1/2	−40.975(11)	0.06649	−81.20
2	0	1/2	1/2	3/2	−30.692(2)	0.40000	0.01
3	2	5/2	5/2	3/2	−27.064(11)	0.13249	−33.07
4	2	5/2	5/2	5/2	−9.415(11)	0.19875	26.07
5	2	3/2	3/2	7/2	−7.846(16)	0.39886	−22.19
6	2	3/2	3/2	5/2	1.587(16)	0.29812	51.32
7	2	5/2	5/2	7/2	6.318(11)	0.26591	50.33
8	**2**	**5/2**	**5/2**	**9/2**	**13.883(11)**	**0.33333**	**−28.13**
9	2	3/2	3/2	3/2	14.702(16)	0.19873	4.92
10	**0**	**1/2**	**1/2**	**5/2**	**20.461(1)**	**0.60000**	**−0.02**
11	2	3/2	3/2	1/2	25.879(16)	0.09974	−66.51
			$(vL) = (00) \to (v'L') = (22)$				
1	2	5/2	5/2	1/2	−41.846(11)	0.06651	−80.80
2	0	1/2	1/2	3/2	−29.338(2)	0.40000	0.01
3	2	5/2	5/2	3/2	−28.592(10)	0.13254	−32.80
4	2	5/2	5/2	5/2	−11.730(10)	0.19881	26.02
5	2	3/2	3/2	7/2	−3.474(16)	0.39892	−22.05
6	2	5/2	5/2	7/2	3.337(10)	0.26595	50.07
7	2	3/2	3/2	5/2	5.582(16)	0.29821	51.07
8	**2**	**5/2**	**5/2**	**9/2**	**10.606(11)**	**0.33333**	**−28.02**
9	2	3/2	3/2	3/2	18.115(16)	0.19881	4.76
10	**0**	**1/2**	**1/2**	**5/2**	**19.559(1)**	**0.60000**	**-0.02**
11	2	3/2	3/2	1/2	28.759(16)	0.09976	−66.32
			$(vL) = (01) \to (v'L') = (11)$				
1	1	3/2	5/2	1/2	−33.061(5)	0.29815	50.33
2	1	3/2	3/2	1/2	−22.787(5)	0.04783	102.72
3	1	3/2	5/2	3/2	−11.612(5)	0.41821	−52.31
4	1	1/2	1/2	3/2	−7.593(11)	0.98593	13.69
5	**1**	**3/2**	**5/2**	**5/2**	**−1.754(5)**	**0.28000**	**−0.00**
6	1	3/2	3/2	3/2	−1.339(5)	0.31375	0.08
7	1	1/2	3/2	3/2	2.913(11)	0.49218	−0.06
8	1	3/2	3/2	5/2	8.519(5)	0.62718	52.39
9	1	1/2	3/2	1/2	12.973(10)	0.49305	−13.44
10	1	3/2	1/2	3/2	21.096(5)	0.09564	−102.97
11	1	3/2	1/2	5/2	30.954(5)	0.89412	−50.66

theoretical results about the electric field gradient at the nucleus of D_2, denoted by q [20–22,24].

The fractional uncertainty of the most recent of these results reported in Ref. [24]—about 0.8×10^{-4}—comes from the fractional uncertainties of the experimental value of d and theoretical value of q, 0.6×10^{-4} and 0.5×10^{-4}, respectively. Hyperfine spectroscopy of the D_2^+ ion offers the opportunity for an independent spectroscopic determination of Q_d. Using the example of the purely rotational $E2$ transition $(vL) = (00) \to (v'L') = (02)$, we discuss the possibility to determine Q_d using the composite frequency method [1,6,23] and the results of the present work as theoretical input, and estimate the accuracy of Q_d that can be achieved this way.

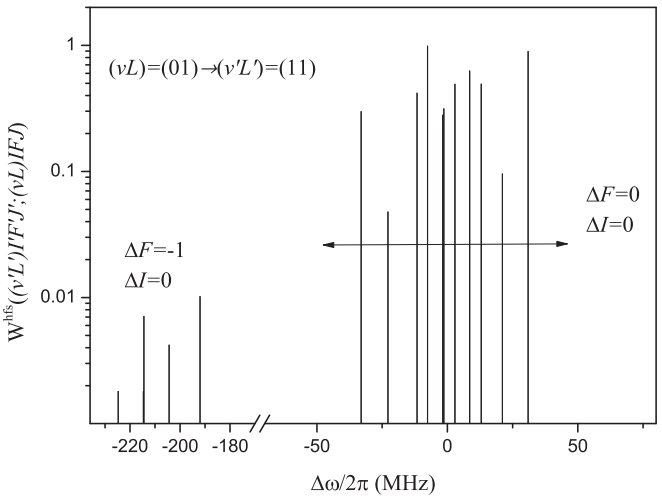

FIG. 4. Hyperfine structure of the $(0, 1) \to (1, 1)\, E2$ vibrational transition line. The intensity of the hyperfine components $\mathcal{W}^{\rm hfs}$ is plotted against the laser frequency detuning $\Delta\omega/2\pi$ from the spin-averaged transition frequency. The spectrum is dominated by the "strong" (favored) components with $\Delta F = \Delta I = 0$, while the intensity of transitions between hyperfine states with different F or I is suppressed by two orders of magnitude. The spectrum also includes a number of "weak" (unfavored) transitions with $\Delta F = +1$, not shown on the plot.

We denote by "composite frequency" $\nu_{\rm c}$ any linear combination of resonance frequencies ν_i of transitions between the rovibrational states (vL) and $(v'L')$ of $D_2{}^+$:

$$\nu_{\rm c} = \sum_{i=1}^{N} x_i \nu_i, \tag{36}$$

where x_i are numerical coefficients, normalized with $\sum_{i=1}^{N} x_i^2 = 1$, whose values are to be determined by imposing appropriate additional conditions.

The "experimental" value of the composite frequency is the linear combination of the experimental data, $\nu_{\rm c}^{\rm ex} = \sum_{i=1}^{N} x_i \nu_i^{\rm ex}$, while the "theoretical" value $\nu_{\rm c}^{\rm th} = \sum_{i=1}^{N} x_i \nu_i^{\rm th}$ is expressed in terms of the difference of the energy levels of the initial (lower) and final (upper) states of the transitions as defined in Eq. (6):

$$\begin{aligned} \nu_i^{\rm th} &= (E^{(v'L')I_i'F_i'J_i'J_{zi}'} - E^{(vL)I_iF_iJ_iJ_{zi}})/h \\ &= \nu_{\rm spin-avg}^{\rm th} + \Delta E^{(v'L')I'F'J'} - \Delta E^{(vL)IFJ}, \\ \nu_{\rm spin-avg}^{\rm th} &= (E^{({\rm diag})v'L'} - E^{({\rm diag})vL})/h. \end{aligned} \tag{37}$$

The quantity $\nu_{\rm c}^{\rm th}$ is a known function of the coefficients of the effective Hamiltonians for the initial and final states E_{in}, E_{in}', $n = 1, ..., 6$, and indirectly of the physical constants involved, including Q_d: $\nu_{\rm c}^{\rm th} = \nu_{\rm c}^{\rm th}(E_{in}, E_{in}', Q_d)$.

The value of Q_d may be determined from the requirement that the theoretical value of the composite frequency be equal to the experimental one,

$$\nu_{\rm c}^{\rm th}(E_{in}, E_{in}', Q_d) = \nu_{\rm c}^{\rm ex} \tag{38}$$

by resolving the latter with respect to Q_d: $Q_d = Q_d(E_{in}, E_{in}', \nu_{\rm c}^{\rm ex})$.

We introduce the notations $\Gamma_{in} = E_n(\partial \nu_i^{\rm th}/\partial E_n)$, $(x \cdot \Gamma_n) = \sum_{i=1}^{N} x_i \Gamma_{in}$ (and similar for the "primed" symbols), where Γ_{in} is the difference of the Γ's defined in Eq. (17) for the final and initial state of the ith transition: $\Gamma_{in} = \Gamma_n^{(v'L')I'F'J'} - \Gamma_n^{(vL)IFJ}$.

The absolute and fractional uncertainties $u(Q_d)$, $u_{\rm r}(Q_d)$ of the quantity Q_d arise from of the experimental uncertainty $u(\nu_{\rm c}^{\rm ex})$ of the experimental composite frequency $\nu_{\rm c}^{\rm ex}$ and from the theory uncertainties of the Hamiltonian coefficients E_n, E_n', $n \leqslant 5$, $\bar{E}_6$, and $\bar{E}_6'$. We denote their fractional uncertainties by u_n, u_n', $n \leqslant 6$, respectively. Under the assumption that these uncertainties are uncorrelated, we obtain the following estimate of the fractional uncertainty $u_{\rm r}(Q_d)$ of Q_d:

$$\begin{aligned} u_{\rm r}(Q_d) &= \frac{u(Q_d)}{Q_d} = \sqrt{u_{\rm r}^{\rm th}(Q_d)^2 + u_{\rm r}^{\rm ex}(Q_d)^2}, \\ u_{\rm r}^{\rm th}(Q_d) &= \frac{\sqrt{\sum_{n=1}^{6} [(x \cdot \Gamma_n) u_n]^2 + [(x \cdot \Gamma_n') u_n']^2}}{|(x \cdot \Gamma_6) + (x \cdot \Gamma_6')|}, \\ u_{\rm r}^{\rm ex}(Q_d) &= \frac{u(\nu_{\rm c}^{\rm ex})}{|(x \cdot \Gamma_6) + (x \cdot \Gamma_6')|}. \end{aligned} \tag{39}$$

Here x denotes the vector $\{x_i\}$. The coefficients x_i are to be determined from the requirement that the fractional uncertainty $u_{\rm r}(Q_d)$ is minimal.

Following the approach developed in Ref. [6], we restrict the search for minima by imposing the constraint $\sum_{i=1}^{N} x_i = 0$ on the components of the vector. This suppresses the contribution from higher-order QED and relativistic spin-independent effects to the composite frequency.

As an illustration of the composite frequency approach, we estimate the accuracy with which the value of Q_d could be retrieved from a measurement of the hyperfine structure of the $E2$ transition $(vL) = (00) \to (v'L') = (02)$. (The numerical estimates for the vibrational transitions $(00) \to (v'2)$, $v' \geqslant 1$ are similar.)

The spectral line has 11 strong (favored) hyperfine components (see Table VI). For the initial state (00), all coefficients E_n but E_3 vanish (see Table I). The numerical values of Γ_{in}', $i = 1, ..., 11$, $n = 1, ..., 6$ and the nonvanishing Γ_{i3} are given in Table VII.

In the absence of real spectroscopy data, we assume in our considerations that the experimental uncertainty of the composite frequency $u(\nu_{\rm c}^{\rm ex}) = \sqrt{\sum_{i=1}^{N} [x_i u(\nu_i^{\rm ex})]^2}$ [where $u(\nu_i^{\rm ex})$ are the uncertainties of the individual hyperfine lines] satisfies $1 < u(\nu_{\rm c}^{\rm ex}) < 170$ Hz and focus our interest to this range; in agreement with Eq. (16) we take $u_n = u_n' = \alpha^2 \approx 5 \times 10^{-5}$. In the range of interest, the uncertainty of Q_d is determined-and limited-by the experimental uncertainty: The contribution of the term $u_{\rm r}^{\rm ex}(Q_d)$ in Eq. (39) exceeds significantly $u_{\rm r}^{\rm th}(Q_d)$ (see Table IX). The dependence of $u_{\rm r}(Q_d)$ on $u(\nu_{\rm c}^{\rm ex})$ is illustrated in Table VIII. The uncertainty $u_{\rm r}(Q_d)$ decreases almost linearly with $u(\nu_{\rm c}^{\rm ex})$, and monotonously with the growth of the number N of hyperfine lines included in the composite frequency $\nu_{\rm c}$. However, beyond $N = 6$ the advantage gained from adding more components ν_i is negligible (see Table VIII). The optimal choice appears to be $N = 6$; Table IX lists the coefficients x_i, $i = 1, ..., 6$ in the optimal linear combination $\nu_{\rm c} = \sum_i x_i \nu_i$, $i \leqslant 6$ for a number of values of $u(\nu_{\rm c}^{\rm ex})$.

TABLE VII. Numerical values of the nonvanishing derivatives $\Gamma_{i\alpha} = E_\alpha(\partial\nu_i/\partial E_\alpha)$ and $\Gamma'_{i\alpha} = E'_\alpha(\partial\nu_i/\partial E'_\alpha)$ for the strong (favored) hyperfine components of the $(00) \to (02)$ transition line, in MHz. To ease comparison with Table III, also given are the correspondent hyperfine shifts from the spin-averaged $E2$-transition frequency $\Delta E^{\rm hfs}/h$, in MHz. $a[b]$ stands for $a \times 10^b$.

i	$\Delta E^{\rm hfs}/h$	Γ'_{i1}	Γ'_{i2}	Γ'_{i3}	Γ'_{i4}	Γ'_{i5}	Γ'_{i6}	Γ_{i3}
1	−40.018	−0.28721[+2]	0.18094[−1]	0.14130[+3]	−0.10064[+2]	0.38755[−2]	−0.23231[−1]	−0.14253[+3]
2	−32.093	−0.32093[+2]	0.00000[+0]	−0.27500[−5]	0.50002[−7]	0.25000[−6]	0.29500[−5]	0.00000[+0]
3	−25.426	−0.20088[+2]	0.14551[−1]	0.13989[+3]	−0.27012[+1]	0.15840[−2]	−0.94920[−2]	0.14253[+3]
4	−12.456	−0.15585[+2]	−0.11915[−1]	−0.21236[+3]	0.17094[+1]	0.10605[−2]	−0.63596[−2]	0.21380[+3]
5	−6.961	−0.85783[+1]	0.82697[−2]	0.13993[+3]	0.42076[+1]	−0.12390[−2]	0.74380[−2]	−0.14253[+3]
6	−2.633	−0.21195[+1]	0.13370[−2]	−0.21107[+3]	−0.32599[+1]	−0.24500[−2]	0.14685[−1]	0.21380[+3]
7	9.461	0.48872[+1]	−0.89350[−3]	0.14122[+3]	0.58717[+1]	−0.24026[−2]	0.14401[−1]	−0.14253[+3]
8	11.084	0.93903[+1]	0.11065[−1]	−0.21103[+3]	−0.10894[+1]	−0.24250[−3]	0.14465[−2]	0.21380[+3]
9	17.331	0.21395[+2]	−0.12809[−1]	0.14228[+3]	−0.37906[+1]	0.13415[−2]	−0.80425[−2]	−0.14253[+3]
10	21.395	0.21395[+2]	0.00000[+0]	0.49999[−5]	0.10000[−6]	−0.60000[−6]	−0.68000[−5]	0.00000[+0]
11	22.814	0.18024[+2]	0.17128[−1]	−0.21244[+3]	0.34302[+1]	0.31675[−2]	−0.18990[−1]	0.21380[+3]

The above numerical estimates allow to outline the perspectives to determine Q_d by means of spectroscopy of $D_2{}^+$.

For an experimental uncertainty $u(\nu_c^{\rm ex}) = 42.4$ Hz, as in the recently reported high-precision pure rotational spectroscopy of HD^+ [6], the resulting fractional uncertainty of Q_d, $u_r(Q_d) \simeq 0.0015$, is nearly an order of magnitude smaller than what was obtained in HD^+.

To distinguish the values of Q_d reported in Refs. [21,22], on the one hand, and in Refs. [20,24], on the other, the fractional uncertainty of Q_d should be $u_r(Q_d) \lesssim 10^{-3}$. Table VIII shows that this could be achieved using the theoretical results of the present work if $u(\nu_c^{\rm ex})$ does not exceed 30 Hz—a level of experimental accuracy that has already been reached in HD^+ spectroscopy, albeit so far only on a single transition [6].

The accuracy of the extracted value of Q_d would become competitive to the most precise available results if $u(\nu_c^{\rm ex})$ could be reduced to the ≈2 Hz range. This is close to the experimental precision needed to extract Q_d by direct comparison of the experimental and theoretical frequency of single hyperfine transitions (see Sec. II C). However, only the composite frequency approach allows to reduce the theoretical error to a correspondingly low level.

It should be stressed that the efficiency of this approach depends on the type of transition: In transitions $(vL) \to (v'L')$ with $\Delta L = 0$ the suppression of the theoretical uncertainty $u_r^{\rm th}(Q_d)$ is less pronounced. Also note that determining Q_d from spectroscopy of HD^+ with an uncertainty comparable to the values in Table VIII would only be possible with a significantly larger number N of hyperfine components of the composite frequency compared to $D_2{}^+$ spectroscopy.

E. Determining the spin-averaged frequency by the composite frequency method

Similar to the above, one may also seek a composite frequency that contains the spin-averaged frequency but minimizes the impact of the theory uncertainties of the HFS coefficients. This concept has been introduced in the experimental work of Ref. [6] and in complementary form in Ref. [23]. For $D_2{}^+$, this approach is particularly simple. As can be seen in Table VII, lines 2 and 10 are practically only sensitive to the coefficient E'_1. Both the initial and final states for these transitions are nearly pure, with strongly suppressed admixture of other states, since the coupling through the terms with E_2, E_3, and E_4 of $H^{\rm eff}$ of Eq. (11) vanishes for $I = 0$, and $|E_{5,6}| \ll |E_1|$. This yields the approximate expressions for the hyperfine shift of energy levels of these states: $\Delta E^{(vL)0FJ} \approx E_1(J(J+1) - F(F+1) - L(L+1))/2$, which are accurate to better than 10^{-5}. Therefore, one can determine the spin-averaged frequency by

$$\nu^{\rm ex}_{\rm spin-avg} = \tfrac{2}{5}\nu^{\rm ex}_2 + \tfrac{3}{5}\nu^{\rm ex}_{10}. \tag{40}$$

The theoretical counterpart of this expression has 0.01 Hz uncertainty coming from the spin structure theory, negligible compared to the uncertainty coming from the QED theory. The same holds for the vibrational transitions $(0, 0) \to (1, 2)$

TABLE VIII. Achievable fractional uncertainty $u_r(Q_d)$ of the electric quadrupole moment of the deuteron Q_d if retrieved from a composite frequency for the $E2$ transition $(00) \to (02)$ versus the number N of hyperfine components involved, for experimental uncertainties $u(\nu_c^{\rm ex})$ between 170 and 1.3 Hz. $a[b]$ stands for $a \times 10^b$.

	Experimental uncertainty $u(\nu_c^{\rm ex})$ (Hz)							
N	169.6	84.8	42.4	21.2	10.6	5.3	2.6	1.3
4	0.57[−2]	0.34[−2]	0.23[−2]	0.19[−2]	0.10[−2]	0.60[−3]	0.44[−3]	0.39[−3]
5	0.53[−2]	0.28[−2]	0.15[−2]	0.85[−3]	0.48[−3]	0.29[−3]	0.16[−3]	0.10[−3]
6	0.52[−2]	0.27[−2]	0.15[−2]	0.80[−3]	0.42[−3]	0.22[−3]	0.12[−3]	0.76[−4]
7	0.51[−2]	0.27[−2]	0.15[−2]	0.79[−3]	0.41[−3]	0.21[−3]	0.12[−3]	0.75[−4]

TABLE IX. Theoretical, experimental, and overall fractional uncertainties $u_r^{th}(Q_d)$, $u_r^{ex}(Q_d)$, and $u_r(Q_d)$ of the deuteron quadrupole moment [see Eq. (39)], and coefficients x_i of the optimal composite frequency ν_c of Eq. (36) for $N = 6$ measured components, as function of the experimental uncertainty $u(\nu_c^{ex})$. $a[b]$ stands for $a \times 10^b$.

$u(\nu_c^{ex})$ (Hz)	$u_r(Q_d)$	$u_r^{ex}(Q_d)$	$u_r^{th}(Q_d)$	Coefficients x_i of the composite frequency ν_c (see Eq. (36))											
169.6	0.52[−2]	0.51[−2]	0.11[−2]	$x_1 =$	0.32087	$x_4 =$	0.14350	$x_5 =$	−0.10214	$x_6 =$	−0.70800	$x_7 =$	−0.21761	$x_{11} =$	0.56338
84.8	0.27[−2]	0.26[−2]	0.91[−3]	$x_1 =$	−0.31117	$x_4 =$	−0.18378	$x_5 =$	0.15051	$x_6 =$	0.72653	$x_7 =$	0.15960	$x_{11} =$	−0.54169
42.4	0.15[−2]	0.14[−2]	0.56[−3]	$x_1 =$	0.28355	$x_2 =$	0.11919	$x_4 =$	0.12758	$x_5 =$	−0.35445	$x_6 =$	−0.69950	$x_{11} =$	0.52363
21.2	0.80[−3]	0.77[−3]	0.22[−3]	$x_1 =$	−0.33803	$x_2 =$	−0.25157	$x_3 =$	0.21766	$x_5 =$	0.27110	$x_6 =$	0.64054	$x_{11} =$	−0.53970
10.6	0.42[−3]	0.41[−3]	0.99[−4]	$x_1 =$	−0.38008	$x_2 =$	−0.24975	$x_3 =$	0.32938	$x_5 =$	0.20048	$x_6 =$	0.61545	$x_{11} =$	−0.51547
5.3	0.22[−3]	0.21[−3]	0.61[−4]	$x_1 =$	−0.39541	$x_2 =$	−0.24740	$x_3 =$	0.37397	$x_5 =$	0.16986	$x_6 =$	0.60123	$x_{11} =$	−0.50225
2.7	0.12[−3]	0.11[−3]	0.54[−4]	$x_1 =$	0.11282	$x_2 =$	0.40157	$x_5 =$	−0.47272	$x_6 =$	−0.61674	$x_9 =$	0.11895	$x_{11} =$	0.45611
1.3	0.76[−4]	0.53[−3]	0.54[−4]	$x_1 =$	0.11188	$x_2 =$	0.40259	$x_5 =$	−0.47320	$x_6 =$	−0.61632	$x_9 =$	0.11976	$x_{11} =$	0.45529

and $(0, 0) \rightarrow (2, 2)$. It is remarkable that only two spin transitions suffice to yield the spin-averaged frequency; this may be a significant advantage compared to HD^+.

IV. CONCLUSION

The present paper reports a series of theoretical results about the spectroscopy of the molecular ion D_2^+, including the most accurate to date calculations of the hyperfine structure of the lower excited rovibrational states with vibrational and rotational quantum numbers $v \leqslant 10$, $L \leqslant 4$. The correct theoretical treatment of the hyperfine structure is essential, considering that the experimental uncertainty of the measurement of the hyperfine structure has already reached the 20-Hz level in one of the molecular hydrogen ions [6].

The paper also presents an evaluation of the hyperfine structure of the $E2$ ro-vibrational transitions and a thorough consideration of the laser polarization effects in the laser spectroscopy of the resolved Zeeman components of the hyperfine transition lines.

The work closely followed but also further developed the formalism of Ref. [13] for the study of the electric quadrupole transition spectrum of H_2^+. The demonstrated efficiency of the composite frequency method underlines the perspectives for precision spectroscopy on D_2^+ in the near future.

Given the expected continued progress of experimental precision in trapped molecular ion spectroscopy, this work provides strong motivation for improving further the theoretical accuracy of the hyperfine coefficients and of the QED energies. Apart from the well-known goals of deuteron-to-electron mass ratio and electric quadrupole moment determination and test of QED, the spectroscopy of D_2^+ specifically opens the possibility of searching for an anomalous force between deuterons [30].

ACKNOWLEDGMENTS

D.B. and P.D. gratefully acknowledge the support of Bulgarian National Science Fund under Grant No. DN 08-17. V.I.K. acknowledges support from the Russian Foundation for Basic Research under Grant No. 19-02-00058-a. S.S., D.B., and V.I.K. acknowledge support from the European Research Council (ERC) under the European Union's Horizon 2020 research and innovation programme (Grant Agreement No. 786306 "PREMOL" ERC-2017-AdG).

[1] S. Schiller, D. Bakalov, and V. I. Korobov, Simplest Molecules as Candidates for Precise Optical Clocks, Phys. Rev. Lett. **113**, 023004 (2014).

[2] J.-P. Karr, H_2^+ and HD^+: Candidates for a molecular clock, J. Mol. Spectrosc. **300**, 37 (2014).

[3] J.-P. Karr, L. Hilico, J. C. J. Koelemeij, and V. I. Korobov, Hydrogen molecular ions for improved determination of fundamental constants, Phys. Rev. A **94**, 050501(R) (2016).

[4] S. Alighanbari, M. G. Hansen, S. Schiller, and V. I. Korobov, Rotational spectroscopy of cold and trapped molecular ions in the Lamb-Dicke regime, Nat. Phys. **14**, 555 (2018).

[5] S. Patra, J.-P. Karr, L. Hilico, M. Germann, V. I. Korobov, and J. C. J. Koelemeij, Proton–electron mass ratio from HD^+ revisited, J. Phys. B: At. Mol. Opt. Phys. **51**, 024003 (2018).

[6] S. Alighanbari, G. S. Giri, F. L. Constantin, V. I. Korobov, and S. Schiller, Precise test of quantum electrodynamics and determination of fundamental constants with HD^+ ions, Nature (London) **581**, 152 (2020).

[7] S. Patra, M. Germann, J.-Ph. Karr, M. Haidar, L. Hilico, V. I. Korobov, F. M. J. Cozijn, K. S. E. Eikema, W. Ubachs, and J. C. J. Koelemeij, Proton-electron mass ratio from laser spectroscopy of HD^+ at the part-per-trillion level, Science **369**, 1238 (2020).

[8] E. Tiesinga, P. J. Mohr, D. B. Newell, and B. N. Taylor, Values of fundamental physical constants, NIST (2019), https://physics.nist.gov/cuu/Constants/index.html.

[9] D. R. Bates and G. Poots, Properties of the hydrogen molecular ion I: Quadrupole transitions in the ground electronic state and dipole transitions of the isotopic ions, Proc. Phys. Soc. A **66**, 784 (1953).

[10] A. G. Posen, A. Dalgarno, and J. M. Peek, The quadrupole vibration-rotation transition probabilities of the molecular hydrogen ion, At. Data Nucl. Data Tables **28**, 265 (1983).

[11] H. Olivares-Pilón and D. Baye, Quadrupole transitions in the bound rotational-vibrational spectrum of the hydrogen molecular ion, J. Phys. B: At. Mol. Opt. Phys. **45**, 065101 (2012).

[12] H. Olivares-Pilón, Quadrupole transitions in the bound rotational-vibrational spectrum of the deuterium molecular ion, J. Phys. B: At. Mol. Opt. Phys. **46**, 245101 (2013).

[13] V. I. Korobov, P. Danev, D. Bakalov, and S. Schiller, Laser-stimulated electric quadrupole transitions in the molecular hydrogen ion H_2^+, Phys. Rev. A **97**, 032505 (2018).

[14] P. Zhang, Z. Zhong, and Z. Yan, Contribution of the deuteron quadrupole moment to the hyperfine structure of D_2^+, Phys. Rev. A **88**, 032519 (2013).

[15] P. Zhang, Z. Zhong, Z. Yan, and T. Shi, Precision spectroscopy of the hydrogen molecular ion D_2^+, Phys. Rev. A **93**, 032507 (2016).

[16] J. F. Babb, The hyperfine structure of the hydrogen molecular ion, Talk at PSAS-2008, University of Windsor, Windsor, Ontario, Canada, July 21–26, 2008, http://web2.uwindsor.ca/psas/Full_Talks/Babb.pdf.

[17] H. A. Cruse, C. Jungen, and F. Merkt, Hyperfine structure of the ground state of para-D_2^+ by high-resolution Rydberg-state spectroscopy and multichannel quantum defect theory, Phys. Rev. A **77**, 042502 (2008).

[18] A. Carrington, C. A. Leach, A. J. Marr, R. E. Moss, C. H. Pyne, and T. C. Steimle, Microwave spectra of the D_2^+ and HD^+ ions near their dissociation limits, J. Chem. Phys. **98**, 5290 (1993).

[19] J. F. Babb, in *Current Topics in Physics*, Vol. 2 edited by Y. M. Cho, J. B. Hong, and C. N. Yang (World Scientific, Singapore, 1998), p. 531, https://doi.org/10.1142/3617.

[20] M. Pavanello, W. C. Tung, and L. Adamowicz, Determination of deuteron quadrupole moment from calculations of the electric field gradient in D_2 and HD, Phys. Rev. A **81**, 042526 (2010).

[21] H. Jóźwiak, H. Cybulski, and P. Wcisło, Hyperfine components of all rovibrational quadrupole transitions in the H_2 and D_2 molecules, J. Quant. Spectrosc. Radiat. Transf. **253**, 107186 (2020).

[22] J. Komasa, M. Puchalski, and K. Pachucki, Hyperfine structure in the HD molecule, Phys. Rev. A **102**, 012814 (2020).

[23] S. Schiller and V. I. Korobov, Canceling spin-dependent contributions and systematic shifts in precision spectroscopy of molecular hydrogen ions, Phys. Rev. A **98**, 022511 (2018).

[24] M. Puchalski, J. Komasa, and K. Pachucki, Hyperfine Structure of the First Rotational Level in H_2, D_2, and HD Molecules and the Deuteron Quadrupole Moment, Phys. Rev. Lett. **125**, 253001 (2020).

[25] D. Bakalov, S. Schiller, and V. I. Korobov, High-Precision Calculation of the Hyperfine Structure of the HD^+ ion, Phys. Rev. Lett. **97**, 243001 (2006).

[26] D. Bakalov, V. I. Korobov, and S. Schiller, Magnetic field effects in the transitions of the HD^+ molecular ion and precision spectroscopy.J. Phys. B: At. Mol. Opt. Phys. **44**, 025003 (2011).

[27] V. I. Korobov, D. Bakalov, and H. J. Monkhorst, Variational expansion for antiprotonic helium atoms, Phys. Rev. A **59**, R919(R) (1999).

[28] See Supplemental Material at http://link.aps.org/supplemental/10.1103/PhysRevA.103.012805 for the numerical data related to the hyperfine structure of the rovibrational states of D_2^+ with $v \leqslant 10$ and $L \leqslant 4$ and the spectrum of $E2$ transitions between them.

[29] R. F. Code and N. F. Ramsey, Molecular-beam magnetic resonance studies of HD and D_2, Phys. Rev. A **4**, 1945 (1971).

[30] E. J. Salumbides, W. Ubachs, and V. I. Korobov, Bounds on fifth forces at the sub-Å length scale, J. Mol. Spectrosc. **300**, 65 (2014).